Received: 18 February 2021 | Revised: 2 September 2021 | Accepted: 27 September 2021

DOI: 10.1111/gbi.12474

ORIGINAL ARTICLE

gebiology WILEY

Microbial chemolithotrophic oxidation of pyrite in a subsurface shale weathering environment: Geologic considerations and potential mechanisms

Stephanie A. Napieralski[1] | Yihang Fang[1] | Virginia Marcon[2,3] | Brandon Forsythe[2] | Susan L. Brantley[2,3] | Huifang Xu[1] | Eric E. Roden[1]

[1]Department of Geoscience, University of Wisconsin-Madison, Madison, Wisconsin, USA

[2]Earth and Environmental Systems Institute, University Park, Pennsylvania, USA

[3]The Department of Geosciences, Pennsylvania State University, University Park, Pennsylvania, USA

Correspondence
Stephanie A. Napieralski and Eric E. Roden, Department of Geoscience, University of Wisconsin-Madison, Madison, WI 53706, USA.
Emails: snapieralski@wisc.edu (SAN); eroden@geology.wisc.edu (EER)

Funding information
University of Wisconsin-Madison; NASA Astrobiology Institute; National Science Foundation, Grant/Award Number: EAR-1239285 and EAR-1331726

Abstract

Oxidative weathering of pyrite plays an important role in the biogeochemical cycling of Fe and S in terrestrial environments. While the mechanism and occurrence of biologically accelerated pyrite oxidation under acidic conditions are well established, much less is known about microbially mediated pyrite oxidation at circumneutral pH. Recent work (Percak-Dennett et al., 2017, *Geobiology*, 15, 690) has demonstrated the ability of aerobic chemolithotrophic microorganisms to accelerate pyrite oxidation at circumneutral pH and proposed two mechanistic models by which this phenomenon might occur. Here, we assess the potential relevance of aerobic microbially catalyzed circumneutral pH pyrite oxidation in relation to subsurface shale weathering at Susquehanna Shale Hills Critical Zone Observatory (SSHCZO) in Pennsylvania, USA. Specimen pyrite mixed with native shale was incubated in groundwater for 3 months at the inferred depth of in situ pyrite oxidation. The colonized materials were used as an inoculum for pyrite-oxidizing enrichment cultures. Microbial activity accelerated the release of sulfate across all conditions. 16S rRNA gene sequencing and metagenomic analysis revealed the dominance of a putative chemolithoautotrophic sulfur-oxidizing bacterium from the genus *Thiobacillus* in the enrichment cultures. Previously proposed models for aerobic microbial pyrite oxidation were assessed in terms of physical constraints, enrichment culture geochemistry, and metagenomic analysis. Although we conclude that subsurface pyrite oxidation at SSCHZO is largely abiotic, this work nonetheless yields new insight into the potential pathways by which aerobic microorganisms may accelerate pyrite oxidation at circumneutral pH. We propose a new "direct sulfur oxidation" pathway, whereby sulfhydryl-bearing outer membrane proteins mediate oxidation of pyrite surfaces through a persulfide intermediate, analogous to previously proposed mechanisms for direct microbial oxidation of elemental sulfur. The action of this and other direct microbial pyrite oxidation pathways have major implications for controls on pyrite weathering rates in circumneutral pH sedimentary environments where pore throat sizes permit widespread access of microorganisms to pyrite surfaces.

KEYWORDS
chemolithotrophy, metagenomics, pyrite, sulfur oxidation, weathering

1 | INTRODUCTION

Pyrite (FeS_2) is commonly observed in sedimentary rocks, for example shales, which comprise an estimated 25% of exposed continental rocks (Amiotte Suchet et al., 2003). Pyrite is also present in anoxic soils and in both freshwater and marine sedimentary environments where conditions are conducive for formation and preservation (Berner, 1984). As such, pyrite is the most abundant sulfide mineral in Earth's crust, and its formation and destruction play a critical role in modern iron and sulfur cycles (Raiswell & Canfield, 2012), as well as in modulation of Earth's O_2 and CO_2 budgets over geologic time (Berner, 2006). The oxidative weathering of pyrite is rapid in near surface environments due to the high reactivity of pyrite in the presence of molecular oxygen. An extensive body of literature exists on the oxidation of pyrite in anthropogenically disturbed systems, including those impacted by mining activities. The rapid exposure of sulfide-bearing rock to atmospheric oxygen results in the generation of large quantities of sulfuric acid, presenting significant environmental concerns including acid rock drainage and mobilization of toxic metals (Blowes et al., 2003). Under acidic conditions, soluble ferric iron acts as dominant oxidant for pyrite, owing to the solubility of Fe(III) at low pH and the rapid reaction of Fe^{3+} ions with pyrite (Moses et al., 1987). It has long been recognized and is well established that microbial communities in acid mine drainage are key in mediating pyrite oxidation by virtue of their ability to aerobically oxidize Fe^{2+} ions released during pyrite oxidation back to Fe^{3+} (Baker & Banfield, 2003; Colmer & Hinkle, 1947). Chemolithotrophic iron and sulfur-oxidizing acidophiles such as *Acidithiobacillus ferrooxidans* and *Acidithiobacillus thiooxidans* can thus effectively accelerate the rate-limiting step of pyrite oxidation by several orders of magnitude at low pH (Singer & Stumm, 1970).

Though a volumetrically large reservoir of pyrite resides in undisturbed sedimentary rock below ground, the mechanism of oxidation of subsurface pyrite is not well understood, particularly with regard to the potential role of microbial activity in oxidation. In such subsurface environments, the pH has the potential to remain largely circumneutral due to the buffering capacity of carbonate and silicate minerals (Nicholson et al., 1988; Vear & Curtis, 1981). While there is a growing body of literature on the circumneutral chemolithotrophic microbial oxidation of pyrite coupled to denitrification (Bosch & Meckenstock, 2012; Haaijer et al., 2007; Jørgensen et al., 2009), fewer studies have examined aerobic oxidation of pyrite by neutrophilic chemolithotrophs. The growth of such organisms has been previously suggested in hydrothermal habitats (Edwards et al., 2003; Wirsen et al., 1993) and subglacial ecosystems (Boyd et al., 2014; Harrold et al., 2015). Only recently, however, has explicit evidence for microbially accelerated aerobic pyrite oxidation at neutral pH been presented (Percak-Dennett et al., 2017). Percak-Dennett et al. (2017) demonstrated sustained enhancement of sulfate release in the presence of a live, natural inoculum over multiple generations in cultures grown on synthetic pyrite. Based upon genomic and geochemical evidence, the authors proposed two potential mechanisms whereby chemolithotrophic microorganisms could accelerate pyrite oxidation. The first mechanism, termed the "sorbed Fe redox cycling model," is based on the model for abiotic oxidation of pyrite at circumneutral pH proposed by Moses and Herman (1991). Here, the cyclic oxidation and reduction of a surface-associated Fe phase couple the successive transfer of pyrite-S electrons to O_2, resulting in the eventual liberation of sulfate. In this case, biological acceleration of pyrite oxidation arises from mineral surface colonization by Fe(II)-oxidizing bacteria (FeOB) that promote the oxidation of sorbed Fe(II) by O_2. An alternative, "polythionate intermediate model" was also proposed by Percak-Dennett et al. (2017), in which chemical reaction of O_2 with pyrite generates partially oxidized sulfur species (e.g., thiosulfate), which are consumed by sulfur-oxidizing bacteria (SOB), thereby accelerating the overall oxidation via Le Chatelier effect. Notably, in the case of the polythionate intermediate model, direct cell-mineral contact is not necessarily required for oxidation of aqueous polythionates. The validity and potential environmental significance of these proposed mechanisms remain an open question, particularly in nanoporous sedimentary materials such as shale where pyrite is commonly hosted.

In the absence of rapid exhumation, either by anthropogenic activity (i.e., mining) or by natural processes (e.g., glacial scouring), pyrite oxidation largely occurs at depth where the circulation of oxidant charged meteoric water leads to the establishment of subsurface reaction fronts. The oxidation of pyrite often occurs as the deepest reaction front in pyrite-bearing rocks (Bolton et al., 2006; Brantley et al., 2013; Littke et al., 1991). Recent work has further confirmed that under modern rates of erosion and atmospheric O_2 concentrations, the oxidation of pyrite in rocks largely occurs below the land surface (Gu, Heaney, et al., 2020). In their study of deep pyrite oxidation at Susquehanna Shale Hills Critical Zone Observatory (SSHCZO), Gu, Heaney, et al. (2020) determined that pyrite oxidation is likely to be transport limited, where diffusion of oxidant into the matrix limits the overall rate of oxidation. Although the nanoporosity of the deep, unweathered Rose Hills Shale at SSHCZO (Jin et al., 2011) precludes direct microbial colonization of a large portion of the disseminated framboidal and euhedral pyrite, the protolith itself is fractured (Brantley et al., 2013). Pyrite oxidation was shown to largely occur within a length scale of centimeters from the fractures in some locations (Gu, Heaney, et al., 2020) where microorganisms could, in theory, reside. It is argued that this pyrite oxidation at depth could be rate limiting with respect to controlling stream incision into the valley (Sullivan, Hynek, et al., 2016). Similarly, previous studies have suggested that microbial pyrite oxidation along fracture planes in receding shale cliffs could contribute to rock weakening (Cockell et al., 2011). SSHCZO thus provides an excellent opportunity to investigate the potential for microbially mediated oxidative weathering of pyrite in shales, and to advance our understanding of microbially catalyzed oxidation of pyrite at circumneutral pH in general. By superimposing the relevant geologic constraints of a fractured subsurface shale on the potential mechanisms of microbially accelerated pyrite oxidation proposed by Percak-Dennett and colleagues (Figure 1), we sought to further test these ideas and assess their potential relevance in situ. In order to allow for cultivation

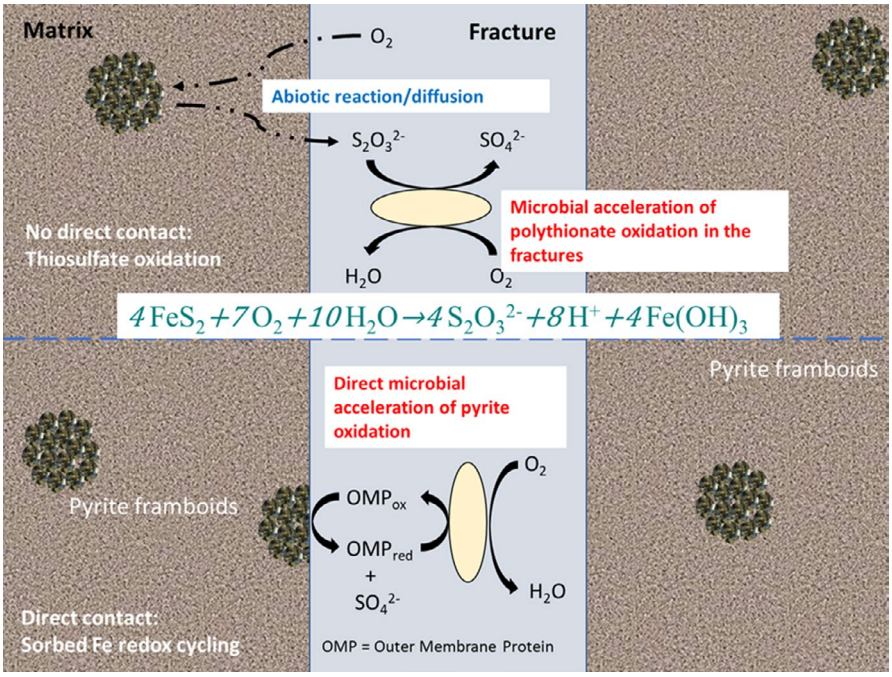

FIGURE 1 Proposed models for microbially mediated circumneutral pyrite oxidation in the shale matrix and fracture network at SSHZO. The indirect polythionate intermediate model (top) allows for microbial colonization of fracture spaces and consumption of abiotically generated polythionates diffusing through the matrix to the fractures. The direct oxidation model (bottom) requires cell–mineral contact and is thus restricted to the matrix–fracture interface

of potentially novel organisms involved in circumneutral pH pyrite oxidation, a supply of specimen pyrite was provided as a growth substrate. In doing so, rather than supplying thiosulfate directly, we were able to interrogate the relevance of the indirect polythionate intermediate model by replicating the likely source of the substrate in situ.

2 | MATERIALS AND METHODS

2.1 | Site description and field sampling

Located in Central Pennsylvania, SSHCZO is a small, forested catchment underlain mostly by shale within the Rose Hill Formation with extensive geochemical and geomorphological data available (Brantley et al., 2013, 2018; Jin et al., 2010, 2014; Ma et al., 2011, 2013; Sullivan, Hynek, et al., 2016; Sullivan, Ma, et al., 2016). Details relevant to this study are summarized briefly here. The Rose Hill Formation is comprised primarily of a tightly folded Silurian age, organic poor grey shale. Primary mineralogy of the protolith has been previously established and is composed of illite (41 wt%), quartz (36 wt%), and chlorite (15 wt%) with trace Fe oxides, pyrite, and carbonate minerals (ankerite and calcite) (Gu, Mavko, et al., 2020; Jin et al., 2010). Pyrite oxidation is observed to be the first reaction to occur in many locations, ca. 15–20 m below land surface under the ridge crests. Sulfuric acid generation from the reaction of downward diffusing O_2 with pyrite reacts with other mineral phases, the first of which is likely to be the carbonate phases. The carbonate reaction thus closely overlies the pyrite reaction front and provides buffering capacity for pyrite oxidation, at least under the northern ridge and near the outlet of the watershed (Brantley et al., 2013; Gu, Mavko, et al., 2020). Several wells have been installed throughout the catchment, including well DC0 on the northern ridge, which was drilled prior to the establishment of the CZO. In August 2017, groundwater from well DC0 (28.65 m depth) was sampled for aqueous chemistry and microbial community analysis. Prior to sampling, DC0 was purged for a total of 35 min as required to obtain 15 min of stable pH (within 0.2 standard units) and temperature (within 0.2°C) Approximately 2.0 L of groundwater was pumped through sterile 0.22-μM filters in duplicate for DNA extraction. Filters were promptly frozen and shipped to UW-Madison on dry ice and stored at −80°C until extraction. Measurements of temperature, conductivity, pH, E_h, dissolved oxygen, and cation concentrations were made as previously described (Sullivan, Hynek, et al., 2016).

2.2 | In situ microcosms

In situ microcosms were prepared with specimen pyrite purchased from Ward's Scientific. Pyrite was hand ground with a mortar and pestle and sieved to 45–106 μm. Ground pyrite was cleaned via ultrasonication and dilute HNO_3 following previously established protocols (McKibben & Barnes, 1986) to remove fine dust and any oxidation rind. In situ microcosms were prepared in ca. 4-inch squares of 23-μm polyester mesh filter screening. A composite mixture of Rose Hill shale previously obtained from drill core was prepared using shale from the deepest sample from boreholes CZMW1-4 (Brantley et al., 2013). Five g of >106 μm fragments of the composite Rose Hill shale and 5.0 g of pure quartz sand (Acros Chemicals, 140–381 μm) were added to each bag. For bags amended with pyrite, 1.0 g of pyrite was added. The bags were then tied closed with stainless steel jewelry wire and autoclaved. In the field, the bags were secured with a stainless-steel carabiner to a stainless-steel wire, which was then lowered down the well to the inferred depth of the pyrite oxidation

front (ca. 23 m) and allowed to incubate in situ for 3 months. Upon removal, each bag was removed from the line and placed into a sterile Whirl-pack bag. Two bags from each treatment (with or without pyrite) were placed on dry ice for DNA extraction and two bags on blue ice for enrichment culturing. Samples were shipped overnight to the University of Wisconsin and samples were placed at −80 and 4°C prior to DNA extraction and culturing, respectively.

2.3 | Enrichment culturing

Enrichment cultures were established using solid mineral substrates to enrich for chemolithotrophic microorganisms. Varying mineralogical conditions were established using the previously prepared (see above) specimen pyrite (0.6 g) and/or 1.0 g of fragmented and sieved (<106 μM) Rose Hills Shale previously obtained from drill core, along with 5 g of quartz sand. Mineral treatments were as follows: Sand only (S), sand with pyrite (S + Py), sand with shale (S + Sh), and sand with pyrite and shale (S + Py + Sh). Shale Hills artificial ground water (SH-AGW) pH 7.0 was prepared based on measured groundwater geochemistry in well DC0 (see Table S1), with final mM concentrations of 0.04 $CaCl_2{\cdot}2H_2O$, 0.035 $MgCl_2{\cdot}6H_20$, 0.01 KH_2PO_4, 0.1 $NaNO_3$, 0.002 $Na_2SiO_3{\cdot}9H_20$, 1.0 $NaHCO_3$, with or without 10-mM piperazine-N,N′-bis(2-ethanesulfonic acid) (PIPES) for buffered (B) and unbuffered (UB) reactors, respectively. The minerals were suspended in 50 ml of SH-AGW in 120-ml culture bottles to allow for a sufficiently large head space for gas exchange, bubbled with N_2 to prevent oxidation during sterilization, stoppered, and autoclaved. After sterilization, the headspace was flushed with sterile air and the cultures were inoculated with ca. 0.5 g of material from pyrite-containing bags previously incubated in situ in well DC0. Abiotic controls were left uninoculated. All conditions (S-B, S-UB, S + Py-B, S + Py-UB, S + Sh-B, S + Sh-UB, S + Py + Sh-B, S + Py + Sh-UB) were performed in duplicate for live inoculated and uninoculated abiotic controls. Cultures were aseptically sampled at time zero and after 7, 14, 21, 35, 49, 63, 77, 91, 105, 126, and 167 days using a syringe and needle. At each sampling time point, a volume of sterile air equal to the volume of culture removed was added to headspace (2 and 4 ml for time points without and with DNA extractions, respectively) to maintain aerobic conditions. Solids and aqueous phases were separated via centrifugation (10,000 RCF, 10 min) for the analyses described below.

2.4 | Analytical procedures

2.4.1 | Aqueous geochemistry

Samples for aqueous SO_4^{2-} were diluted 1:5 for analysis by ion chromatography (IC, Dionex Model ICS-110). Total tetrathionate and thiosulfate were determined colorimetrically using the alkaline cyanolysis method described in (Nor & Tabatabai, 1975) scaled to accommodate a smaller volume of sample (1.0 ml). Aqueous phase samples were diluted 1:6 in 5 mM HNO_3 and filtered (0.22 μm) prior to the determination of major cation (Ca, K, Mg, Na) concentrations via inductively coupled plasma optical emission spectrometry (ICP-OES). Aqueous silicon was determined colorimetrically on 1:10 dilutions using the heteropoly blue method (Clesceri et al., 1998).

2.4.2 | Solid-phase geochemistry

Mineral solids were extracted for 24 h in 5.0 ml 0.5 M HCl on an orbital shaker. After extraction, the mixture was centrifuged and the concentration of Fe(II) was determined by the standard ferrozine assay (Stookey, 1970). Fe(Total) concentrations in the same extracts were similarly determined after the addition of hydroxylamine HCL.

2.4.3 | ATP analysis

0.5 ml of whole culture (solid and aqueous) was placed into 0.25 ml of 20 mM ice cold EDTA, vortexed at maximum speed, and immediately frozen at −80°C. For analysis, samples were thawed, vortexed again, and centrifuged to recover the aqueous phase. ATP content was determined via luminescence using BacTiter-Glo (Promega) with calibration to a standard curve.

2.4.4 | Microscopy

Whole culture aliquots from day 77 were stained using SYTO® Green and microbe–mineral interactions were examined using epifluorescence microscopy. For analysis of associated mineralogical changes, initial pyrite and mineral solids from the final time point (167 days) were dropped onto a carbon tape and carbon coated. Samples were imaged using a Hitachi S-3400 Scanning Electron Microscope (SEM) equipped with an Energy dispersive X-ray spectroscopy (EDS) detector. Transmission electron microscopy (TEM) analysis was conducted at the Material Science and Engineering Department in University of Wisconsin–Madison using a Tecnai T12 with a 120-kV acceleration voltage. TEM imaging and selected area electron diffraction data were collected by a 4k Gatan Ultrascan CCD. Pyrite grains were manually selected from the cultured materials, suspended in acetone, and cleaved in agate mortar. The cleaved samples were then dropped onto the carbon film 300 mesh copper grid. Compositions were measured by the Thermo Scientific X-ray energy dispersive spectroscopy (EDS).

2.5 | DNA extraction, sequencing, and analysis

2.5.1 | DNA extraction

DNA was extracted from in situ microcosms and enrichment culture solids for days 21, 77 and 167 according to previously described

SDS-based extraction protocols (Zhou et al., 1996). Due to low DNA yields from in situ bag material, 8 0.5 g aliquots were extracted to obtain a sufficient mass of DNA for shotgun metagenomic sequencing. Replicate extracts were pooled and cleaned using Zymo Clean and Concentrator-5 (Zymo Research). Groundwater DNA was extracted from filters by slicing the filter into small pieces with a sterile razor, transferring the small pieces to a 2.0-ml screw-top microcentrifuge tube containing ca. 0.25 ml of 0.1-mm zirconium beads. 0.5 ml of extraction buffer from Zhou et al. (1996) and 10 mg/ml of proteinase-K were added. Samples were incubated on a head block (37°C) with gentle agitation for 1 h. 0.5 ml of phenol-chloroform-isoamyl alcohol (25:24:1) was then added to digest the filter and the tube was bead beat for 1 min. DNA was then isolated following the standard phenol-chloroform-isoamyl alcohol (25:24:1) extraction and recovered via precipitation at −20°C in two volumes of ethanol.

2.5.2 | 16S rRNA gene amplicon sequencing and analysis

DNA was submitted to the University of Wisconsin-Madison Biotechnology Center (UWBC) for Illumina MiSeq 2 × 300 paired end sequencing of the V4 region of the 16S rRNA gene. Sequencing data were processed using The Quantitative Insights into Microbial Ecology (QIIME) pipeline version 1.9.1 (Caporaso, Kuczynski, et al., 2010). Raw reads were quality filtered to remove low quality and ambiguous sequences using default QIIME parameters prior to assembly of paired ends using fastq-join (Aronesty, 2013). Chimeric sequences were identified and discarded via de novo and reference-based detection using USEARCH v. 6.1 (Edgar, 2010) and the SILVA ribosomal RNA database (Quast et al., 2013). Operational taxonomic units (OTUs) were identified by de novo clustering (0.97 threshold). Taxonomy was assigned to OTUs a via alignment against the SILVA database using PyNAST (Caporaso, Bittinger, et al., 2010).

2.5.3 | Metagenomic assembly and annotation

Aliquots of DNA in situ mineral incubations and the final time point (167 days) of enrichment cultures were submitted to UWBC for metagenomic library preparation and 2 × 250 paired end sequencing on the Illumina HiSeq 2500 Rapid platform. A metagenomic library for a single-pooled sample of groundwater DNA was sequencing using MiSeq 2 × 250. Raw metagenomic reads from all samples were quality filtered using the default parameters of Trim-Galore prior to concatenation and coassembly using MegaHit (Li et al., 2015). Metagenome-assembled genomes (MAGs) were obtained from the coassembly using the Bin Refinement module within metaWRAP (Uritskiy et al., 2018) with initial binning output from MetaBAT2 (Kang et al., 2019), MaxBin2 (Wu et al., 2015), and CONCOCT (Alneberg et al., 2014). The quality and completion of individual MAGs as well as putative taxonomy were assessed by CheckM (Parks et al., 2015). Relative abundance of each MAG across each sample in the coassembly was determined using the Bin Quantification module of metaWRAP. Open reading frames were predicted using Prodigal (Hyatt et al., 2010) and functionally annotated using Prokka (Seemann, 2014). Extracellular electron transfer and sulfur oxidation pathways were identified as previously described (He et al., 2017; Watanabe et al., 2019). Maximum likelihood phylogenetic trees in were constructed PhyML 3.0 (Guindon et al., 2010) with the LG substitution model (Le & Gascuel, 2008) for putative lithotroph MAGs using the concatenated alignments of conserved phylogenetic markers obtained from CheckM. All sequencing data generated in this study have been deposited in The National Center for Biotechnology Information under the BioProject Number PRJNA692452.

2.5.4 | Searching for novel pathways for pyrite oxidation

The MAG (*Thiobacillus* related; see below) found to be most abundant across pyrite oxidizing enrichment culture metagenomes was further interrogated to uncover novel potential mechanisms for the oxidation of pyrite, which may involve the extracellular metabolism of pyrite-S. The subcellular location of all MAG proteins was predicted using Cello (Yu et al., 2006). Proteins predicted to be outer membrane associated or extracellular were further examined for genomic proximity to known S-oxidation pathways. Potential homologs to the identified proteins of interest were found by a BLASTp search (Altschul et al., 1990) of the NCBI database of nonredundant proteins. Homologous sequences were aligned using MUSCLE (Edgar, 2004) and conserved motifs visualized with WebLogo 3 (Crooks et al., 2004). Putative structures of proteins of interest were modeled using Phyre2 (Kelley et al., 2015).

3 | RESULTS

3.1 | Groundwater geochemistry and microbial community composition

The geochemistry of groundwater at site DC0 and other locations at SSHCZO has been previously characterized (Sullivan, Hynek, et al., 2016; Sullivan, Ma, et al., 2016). Samples for groundwater geochemistry and microbial community composition were also collected in this study at the time of in situ mineral deployment in August 2017. The chemistry of the groundwater collected during mineral deployment (Table S1) suggested that downhole fluids from a mixture of redox conditions were obtained during sampling by peristaltic pump: the combination of low but measurable dissolved oxygen (0.035 mM), substantial levels of dissolved iron (0.029 mM), and E_h of −180 mV is highly suggestive of redox disequilibrium. These results are not surprising given that (i) an oxidation-reduction front is known to exist at SSHCZO based on prior aqueous and solid-phase geochemical distributions at various locations within the watershed (Brantley et al., 2013; Sullivan,

Hynek, et al., 2016; Sullivan, Ma, et al., 2016); and (ii) the well cased at DC0 such that mixing of fluids from different depths likely took place during peristaltic pump sampling of the 7.6 cm-diameter well. The minerals were deployed 1–2 m below the groundwater surface, and we thus assume that they were exposed to some dissolved O_2 during the 3-month incubation period. Nevertheless, the microbial community in the groundwater sample and the in situ-incubated minerals (Tables S2 and S3, respectively) showed evidence of putative anaerobic heterotrophic taxa, notably Fe(III)-reducing *Geobacteraceae* as well as other organisms related to known anaerobic heterotrophic taxa (e.g., *Thermodesulfovibrionaceae*, *Clostridiaceae*, *Commononaceae*). The proliferation of Fe(III) reducers makes sense assuming Fe(II) oxidation (e.g., in the upper regions of the well) produces an ongoing supply of fresh Fe(III) oxides, which were visibly evident both on the mineral bags and in groundwater filters. In addition, the minerals were also colonized by organisms related to known microaerophilic, Fe(II)-oxidizing organisms from the genera *Gallionella* and *Crenothrix* (Emerson et al., 2010), which suggests that groundwater at DC0 supports the activity of both heterotrophic and chemolithotrophic microorganisms. Due to the well specific conditions of the in situ incubations (e.g., redox fluctuations, steel casing, and potential organic matter entry from the well top), which are not representative of the Rose Hills unit as a whole, for the purposes of this paper, the colonized minerals simply served as an inoculum for pyrite-oxidizing enrichment cultures, and we make no attempt to explicitly link the organisms and activities that arose in those cultures to their absolute mineral weathering activity in situ.

3.2 | Enrichment culture geochemistry

3.2.1 | pH

Solution pH declined from ca. 7.0 to an average of 6.0 and 5.7 in the abiotic and live buffered sand + pyrite (S + Py-B) reactors, respectively (Figure 2a). In the absence of buffer (S + Py-UB), pH declined rapidly from 7.8 to a final average values of 3.5 and 4.4 for abiotic and biotic sand plus pyrite reactors (Figure 2b). pH remained within 0.5 units of the initial value in the buffered, shale-amended (S + Sh-B, S + Py + Sh-B) reactors, declining slightly to 7.1 in the live pyrite system (Figure 2c). In the unbuffered shale-amended reactors, pH declined slightly in the presence of pyrite (S + Py + Sh-UB) and remained unchanged at 7.5–7.8 in its absence (S + Sh-UB) (Figure 2d).

3.2.2 | HCl-extractable Fe

Iron oxidation was observed in all reactors, with the Fe(II)/Fe(total) ratio declining across all treatments. However, no significant differences were observed in the Fe(II)/Fe(total) ratio between the live inoculated and sterile abiotic control reactors for each treatment over the course of the experiment (Figure S1).

3.2.3 | Sulfate

Sulfate generation was enhanced in the presence of a live inoculum relative to sterile controls under all conditions tested (Figure 2e–h). Initial biotic rates of reaction (0–35 days) were 1.9–3.4-fold greater than abiotic rates in the four reaction systems, and total sulfate release over the 167-d incubation period was 1.2 to 4.7-fold higher in the biotic reactors (Table 1). Only small amounts of sulfate were generated from the oxidation of residual pyrite in the inoculum ("Live No Pyrite" in Figure 2), indicating that most of the sulfate release in the pyrite-amended reactors came from oxidation of the added (ca. 200 mmol S L^{-1}) pyrite. The entire range of sulfate release values correspond to oxidation of 0.31–2.4% of the added pyrite-S.

3.2.4 | ATP

The ATP content of the live reactors was maximal at the start of the incubation and declined over time in all reactors (Figure 2i–l); ATP was near to or below detection in the uninoculated controls. ATP levels were similar in the pyrite-containing and pyrite-free buffered reactors (Figure 2i,k), which suggests that any cell growth associated with biologically mediated pyrite oxidation in these reactors (Figure 2e,g) was insufficient to keep up with biomass loss upon addition of the inoculum to the reactors. ATP levels were generally lower in the unbuffered pyrite-containing versus pyrite-free reactors (Figure 2j,l). In the case of the shale-free systems (Figure 2j), the rapid decline in ATP during the first few weeks of incubation can be explained by the precipitous drop in pH (Figure 2b) that took place in conjunction with pyrite oxidation.

3.2.5 | Polythionates

Polythionates (sum of thiosulfate and tetrathionate; see Section 2.4.1) accumulated in the abiotic pyrite-containing reactors (Figure 2m–p) but remained near or below detection in the pyrite-free reactors. Polythionates were consistently low in the live S + Py reactors (Figure 2m–n) and consumed over time in the S + Sh + Py reactors (Figure 2o–p). The onset of polythionate accumulation in the live unbuffered S + Py reactors (Figure 2n) was associated with rapid decline in pH and ATP content (see above), signaling a shift from biotic + abiotic to abiotic-only pyrite oxidation.

3.2.6 | Cations and silica

Accumulation of aqueous cations and silica were used as an indicator of pyrite oxidation-driven dissolution of shale mineral phases, i.e., shale either present in the inoculum, or added separately (in addition to the inoculum) to the reactors. Ca release in particular was assumed to primarily signal the dissolution of carbonate phases (ankerite + calcite) present in samples of Rose

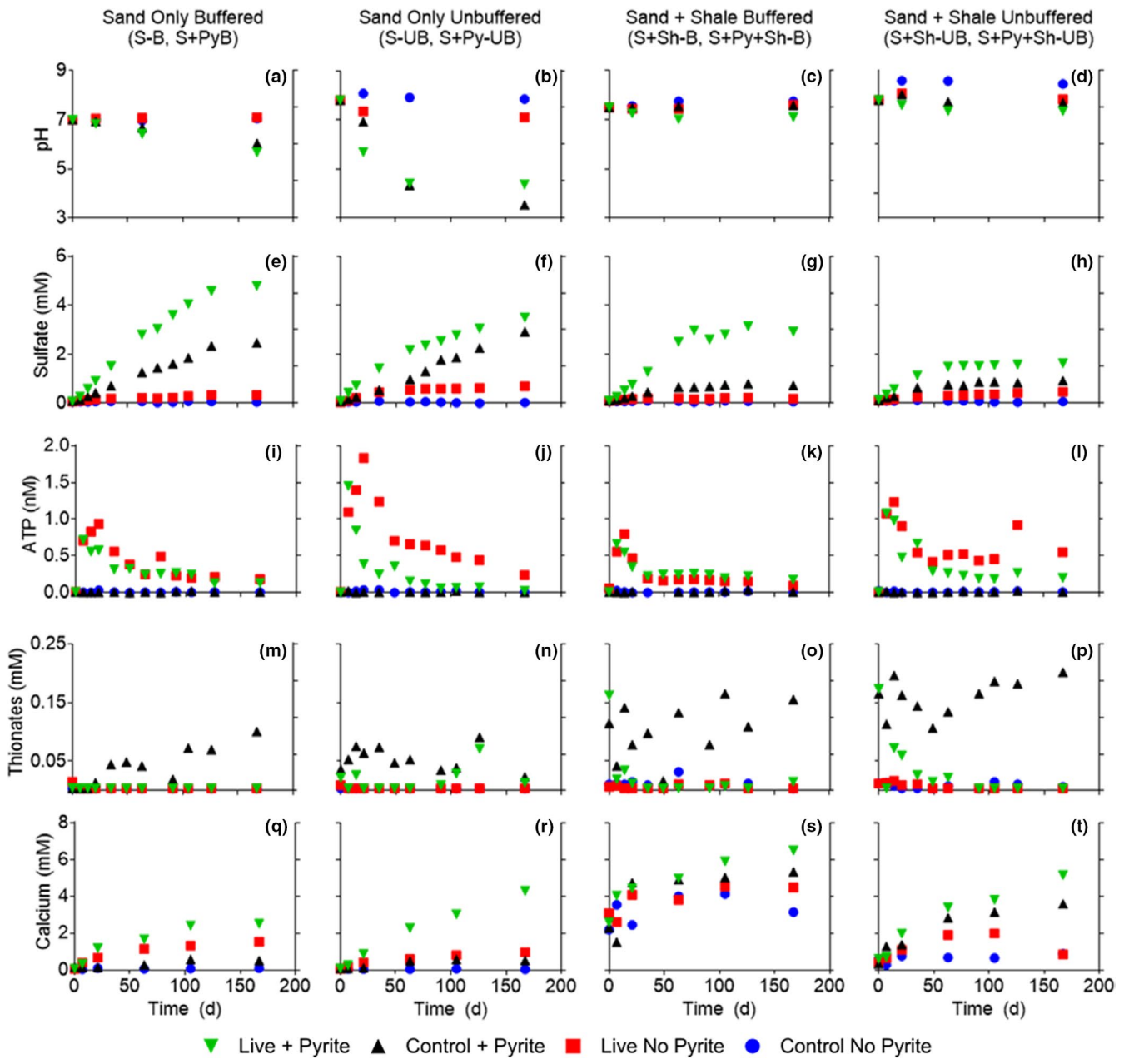

FIGURE 2 Average pH (a–d), sulfate concentration (e–h), ATP content (i–l), total polythionate (m–p), and calcium concentration (q–t) in duplicate reactors for each experimental condition

Hill Shale from depth used to establish the enrichment cultures (Brantley et al., 2013; Jin et al., 2010). Mg release was likely influenced by dissolution of both carbonate and silicate phases, whereas Si and K (not present in carbonate minerals) were assumed to be indicators of silicate dissolution. Ca release was stimulated dramatically by microbial activity in pyrite-amended reactors that did not receive additional shale (Figure 2q,r). Some of this increase could be attributed to biotic and/or abiotic oxidation of pyrite in the inoculum (see Figure 2e,f), as there was a distinct increase (particularly in the buffered reactors) in Ca in the inoculated pyrite-free reactors. Ca levels were higher across the board in the buffered shale-amended reactors (Figure 2s), indicating dissolution of carbonate (i.e., by maintenance of near-neutral solution pH by the buffer) regardless of the presence of pyrite oxidation activity (i.e., elevated Ca levels are also observed in pyrite free reactors). Such dissolution thus masked the distinction between the effects of biotic versus abiotic pyrite oxidation, although final Ca levels were maximal in the buffered live pyrite-amended reactors. In contrast, Ca release was stimulated in the, unbuffered, pyrite-containing shale-amended reactors relative to those lacking pyrite (Figure 2t), although here again some of this increase could be attributed to oxidation of pyrite in the inoculum, as there was also an observable increase in Ca in the live no pyrite reactors. Mg and K showed patterns of release generally analogous to Ca (Figure S2A–H), whereas net Si release occurred only in the shale-free reactors (Figure S2I–L).

TABLE 1 Sulfate releases rate over the first 35 days of incubation

	35-day sulfate release (mM day^{-1})[a]	R^2	Rate fold increase	Initial sulfate (mM)[b]	Final sulfate (mM)[b]	Total sulfate released (mM)[b]	Total release fold change
Sand only buffered							
Live + Py	0.042 ± 0.001	0.9934	2.328	0.085 ± 0.0005	4.794 ± 1.523	4.709 ± 1.522	1.988
Control + Py	0.018 ± 0.0001	0.9798		0.098 ± 0.009	2.466 ± 0.128	2.369 ± 0.119	
Sand only unbuffered							
Live + Py	0.034 ± 0.041	0.9907	2.624	0.086 ± 0.004	3.502 ± 0.688	3.416 ± 0.692	1.203
Control + Py	0.013 ± 0.001	0.9877		0.084 ± 0.022	2.923 ± 1.012	2.839 ± 0.990	
Sand + shale buffered							
Live + Py	0.034 ± 0.001	0.9916	3.431	0.110 ± 0.013	2.929 ± 0.583	2.819 ± 0.596	4.657
Control + Py	0.001 ± 0.001	0.9481		0.117 ± 0.002	0.722 ± 0.156	0.605 ± 0.154	
Sand + shale unbuffered							
Live + Py	0.028 ± 0.001	0.9965	1.897	0.158 ± 0.054	1.630 ± 0.192	1.475 ± 0.138	1.853
Control + Py	0.015 ± 0.004	0.6793		0.125 ± 0.027	0.921 ± 0.810	0.796 ± 0.783	

[a]From linear regression of sulfate concentrations over 35 days for individual reactors and error of the slope.
[b]Average ± range of duplicate reactors.

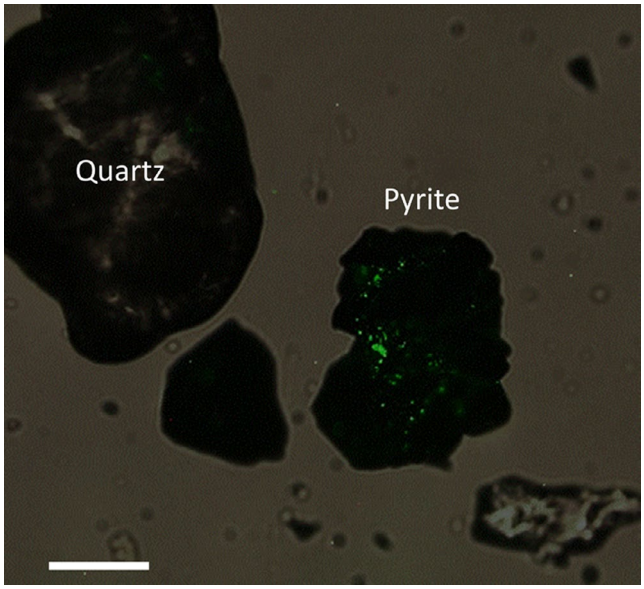

FIGURE 3 Composite (epifluorescence and light) image of SYTO stained microbially colonized pyrite grains after 77 days of incubation. Cells are preferentially adhered to pyrite surfaces rather than quartz grains or in background medium. Scale bar equals 20 μM

3.3 | Microscopy and Mineralogical Alteration

Epifluorescence microscopic analysis from day 105 of the incubation demonstrated a close association of microbial cells with pyrite surfaces. Cells appeared to preferentially colonize pyrite surfaces (opaque under light microscopy), as minimal fluorescence was observed on quartz surfaces (nonopaque) or in bulk solution (Figure 3). Under SEM, initial pyrite surfaces were clean, smooth, and free of any oxide coatings; EDS showed an average weight percent of 52.2% S and 47.8% Fe (Figure S3). Significant alteration of the pyrite surfaces as well as depletion in solid-phase S (final average 36.8% S) was observed after 167 days of both biotic and abiotic incubation. Morphological differences in the altered pyrite surfaces were observed across culturing conditions. In the absence of shale, both buffered and unbuffered uninoculated control pyrite surfaces showed the presence of a lawn of porous, needle-like oxides with morphology consistent with goethite. In live unbuffered S + Py reactors, pyrite surfaces were coated with a smoother, apparently amorphous Fe-oxide coating (Figure 4) with only occasional goethite crystallites. TEM analysis confirmed the presence of goethite on uninoculated control pyrite surfaces, and the presence of amorphous coatings on the biologically altered pyrite (Figure S3). When shale was present, the extensive covering of goethite-like needles was not observed under any experimental condition. Rather, the surfaces appear to be covered in smooth, amorphous coatings, less porous than the needle-like lawn observed under abiotic conditions in the absence of shale (Figure 5).

3.4 | Microbial communities in enrichment cultures

16S rRNA gene amplicon analysis of microbial communities in the pyrite-containing enrichment cultures, both S + Py and S + Py + Sh, revealed a predominance of organisms from the genus *Thiobacillus* (Figure 6, medium blue). In the absence of a pyrite, the most dominant genus was the *Pseudomonas* (Figure 6, brown), a well-known heterotrophic taxon (Moore et al., 2006) that was previously shown to extensively colonize minerals incubated in situ in groundwater (Converse et al., 2015). However, *Thiobacillus* was also observed at elevated abundance in one replicate of S-only and S + Sh reactors,

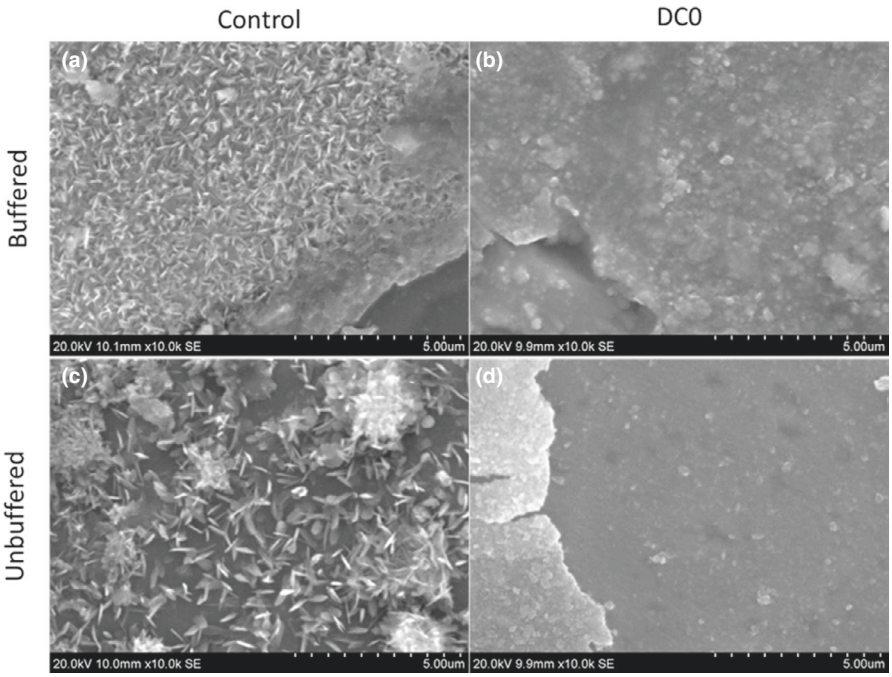

FIGURE 4 SEM images of pyrite grains from S + Py reactors after abiotic incubation (a and c) and incubation with a live inoculum (B and D) for buffered (A and B) and unbuffered (c and d) reactors. Note the presence of discrete Fe oxide nanocrystals in the abiotic systems, which were much less abundance in the live cultures

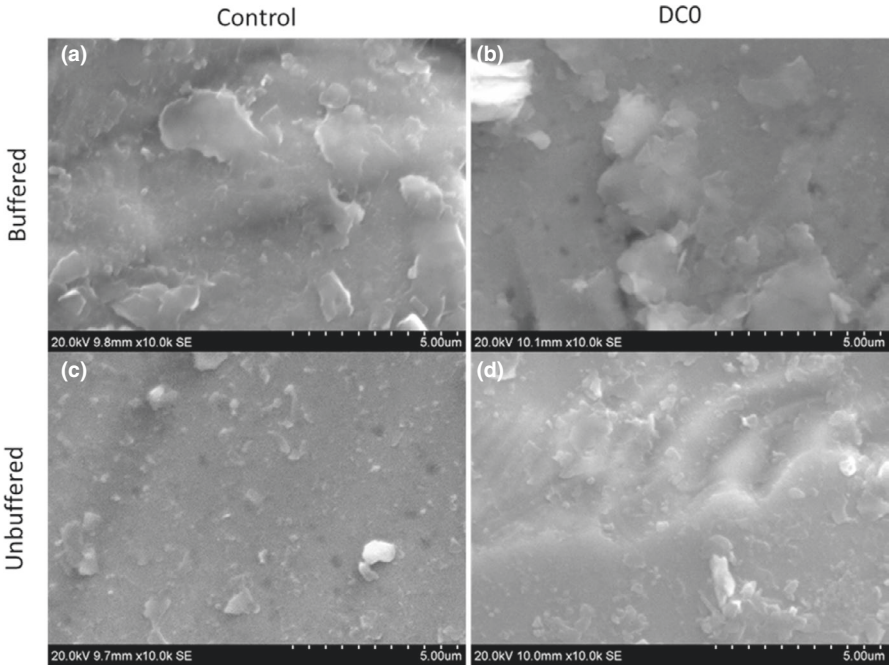

FIGURE 5 SEM images of pyrite grains from S + Py + Sh reactors after abiotic incubation (a and c) and incubation with a live inocula (b and d) for buffered (a and b) and unbuffered reactors. Note the difference in surface morphology and lack of crystalline phases in the abiotic control relative to S + Py reactors

which displayed some release of sulfate. These observations (small differences in sulfate release and differences in microbial communities between replicates of S and S + Sh reactors) are best explained by the oxidation of residual pyrite in the inoculum, which may have been more abundant in one replicate versus another despite our best attempts at homogenization prior to inoculation of duplicate reactors. The extent to which *Thiobacillus* dominated the S + Py and S + Py + Sh 16S rRNA gene amplicon libraries was variable among individual reactors and time, with the highest representation (92.7%) at day 77 in S + Py-B reactors. Contrasting trends in the temporal abundance of *Thiobacillus* were observed in unbuffered and buffered reactors, with a decrease in abundance over time in the unbuffered reactors.

3.5 | Metagenomic analysis of putative litho(auto)trophic pathways

A total of 460 MAGs were obtained from the metagenomic coassembly of the colonized minerals, ground water, and enrichment cultures. Of the 460 MAGs obtained, 157 were determined via CheckM to be of high quality (>90% complete and <5% contamination). A full

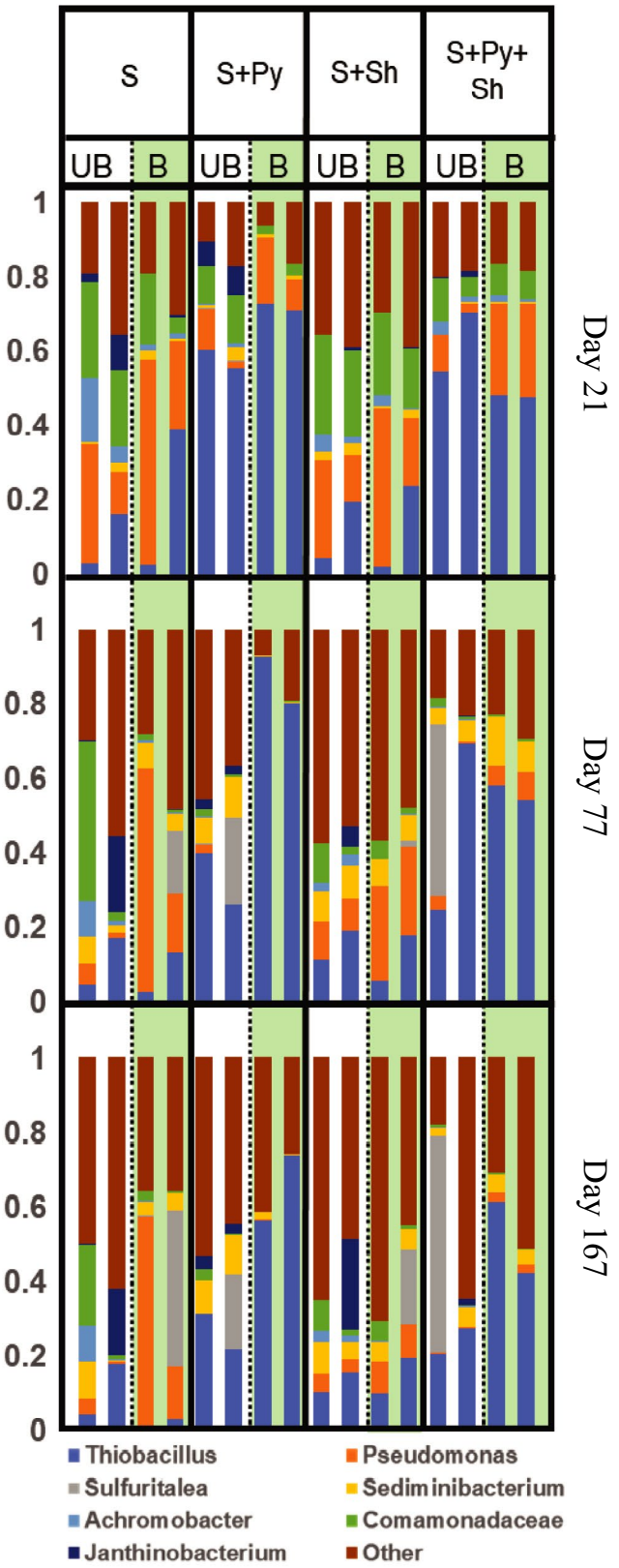

FIGURE 6 16S rRNA gene amplicon sequencing results showing the relative abundance of the dominant genera for each duplicate reactor after 21 (top), 77 (middle), and 167 (bottom) days of incubation for sand (S), sand + pyrite (S + Py), sand + shale (S + Sh), and sand + pyrite + shale (S + Py + Sh)-amended cultures. Buffered (B) and unbuffered (UB) reactors are delimited by a dashed line for each mineral treatment, with buffered reactors shaded in green. Genus or family (when lower taxonomic resolution was not available)-level classification is indicated by the color in the legend, with *Thiobacillus* appearing medium blue at the bottom of each stack

list of the 460 MAGs and associated quality metrics and contained taxonomy as determined via CheckM is provided in the supplemental files. Putative extracellular electron transfer (EET) pathways involved in Fe(II) oxidation were identified in 14 of the 460 MAGs. Homologs to the Cyc2-type iron oxidation pathway originally recognized in *A. ferrooxidans* (Appia-Ayme et al., 1999) were identified in five of the putative FeOB MAGs. The outer membrane-bound c-type monoheme cytochrome Cyc2 acts as a Fe(II) oxidase, transferring electrons to the inner membrane for energy generation via periplasmic electron carriers including Cyc1 (Castelle et al., 2008). Cyc2-type EET systems have subsequently been shown to be widely distributed in the genomes of neutrophilic FeOB (He et al., 2017), where its activity has been recently verified via meta-omics (McAllister et al., 2020) and implicated in the oxidative metabolism of solid-phase Fe minerals (Napieralski et al., 2019). The remaining nine putative FeOB MAGs contained homologs to the MtoABCD EET system (Emerson et al., 2013; Liu et al., 2012). The core proteins of this pathway include the decaheme c-type cytochrome MtoA, which is inserted into the β-barrel porin MtoB, forming an outer membrane spanning electron conduit. Electrons are then delivered to the inner membrane cytochrome MtoC by the periplasmic cytochrome MtoD (He et al., 2017).

Of the 460 MAGs, 49 contained ORFs predicted to encode genes for three essential proteins of the widely distributed sulfur oxidation pathway Sox, including the heterodimeric c-type cytochrome SoxAX, the SoxXY carrier complex, and the sulfate thiohydrolase SoxB (Friedrich et al., 2001). During the oxidation of thiosulfate, SoxAX oxidatively links a thiosulfate molecule to a cysteine residue of SoxY. The sulfane sulfur is then hydrolyzed to sulfate by SoxB (Friedrich et al., 2001; Watanabe et al., 2019). The hydrolysis of SoxYZ by SoxB leaves cysteine persulfide on SoxY. The sulfur dehydrogenase SoxCD, necessary for the oxidation of the sulfane sulfur carried by SoxXY was identified in 36 of the 49 MAGs containing SoxXYAB. Alternatively, in some organisms lacking SoxCD, including *Thiobacillus denitrificans* (Beller, Chain, et al., 2006; Beller, Letain, et al., 2006), a reversely operating sirohaem dissimilatory sulfite reductase (DsrAB (Dahl et al., 2005; Pott & Dahl, 1998)) is employed. A complete reverse Dsr pathway (rDsrABCEFHJKLMNOPRS) was identified in seven of the MAGs containing SoxXYAB. Alternatively, a recently recognized heterodisulfide reductase (Hdr) pathway was identified (Koch & Dahl, 2018) in organisms lacking SoxCD and was identified in eight of the MAGs containing SoxXYAB. Both Dsr and Hdr pathways also require the presence of a membrane-bound sulfite oxidation enzyme, SoeABC (Dahl et al., 2013). SoeABC is conserved in genomes of organisms employing Dsr and Hdr pathways (Watanabe et al., 2019), and accordingly present in all MAGs containing Dsr and Hdr-based S-oxidation pathways.

Of the 63 MAGs that contained putative Fe or S oxidation pathways, a further 28 of them also contained a complete set of genes for inorganic carbon fixation via the Calvin cycle, indicating an ability to grow chemolithoautotrophically. A summary of the distribution of chemolithoautotrophic pathways is provided in Figure 7 with abundances reported across metagenomes in log genome copies per million reads. The majority of the putative lithoautotrophs belong to the class β-proteobacteria, with only four falling within the α-proteobacteria. Both FeOB and SOB were detected across all samples. In the groundwater metagenome (DC0-GWb), two chemolithoautotrophic MAGs are particularly abundant: a putative *Rhodocyclaceae* with both MtoABCD and Sox-Hdr-Soe S-oxidation pathways, and a putative *Comamonadaceae* containing c-Sox, which are the third and sixth most abundant MAGs found in the groundwater, respectively. Chemolithoautotrophic MAGs across in situ mineral-colonized metagenomes (DC0-1 through DC0-6) are also well represented, though the most abundant MAGs across these samples tend to be anaerobic Fe and S-reducing taxa, particularly *Geobacter* and S-reducing *Nitrospiraceae* (Table S5). The differential abundance of the putative lithoautotrophs indicates a strong enrichment for SOB in all pyrite-oxidizing enrichment culture metagenomes, relative to both the groundwater and in situ microcosm metagenomes as evidenced by the high abundance of bins 449 and 12, which both contain Sox pathways. Particularly abundant across all pyrite-amended cultures is MAG 449 (bin 449, Figure 7), which is tentatively identified as belonging to the genus *Thiobacillus* and contains the Sox-Hdr-Soe pathway for S-oxidation.

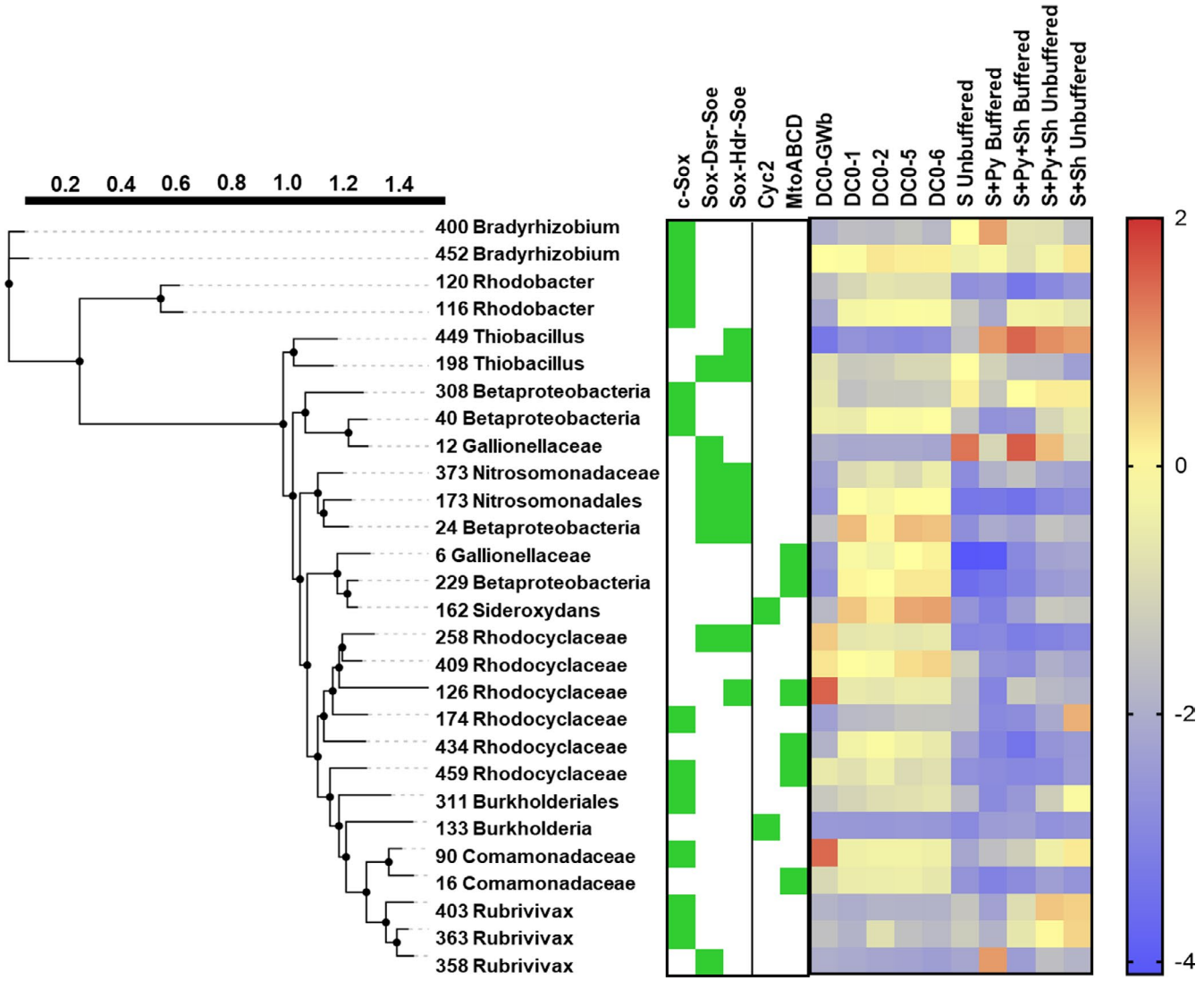

FIGURE 7 Heat map indicating the putative taxonomy and abundance (log genome copies per million reads) of chemolithoautotrophic MAGs obtained from the metagenomic coassembly across all samples in the coassembly (Groundwater; DC0-GwB, in situ mineral deployments; DC01-6 and enrichment cultures for which metagenomic library preparation was successful). The presence of each lithotrophic pathway for either S oxidation (c-Sox, Sox-Dsr-Soe, and Sox-Hdr-Soe) or Fe oxidation (Cyc2 and MtoABCD) in each MAG is indicated by a green square. For clarity, only MAGs containing either an Fe or S oxidation pathway as well as a full CO_2 fixation pathway are shown

3.5.1 | Identification of potential novel pathways

As the most dominant MAG in pyrite-oxidizing enrichments, MAG 449 was further interrogated to uncover potential mechanisms for pyrite oxidation, including the potential for utilization of extracellular reduced sulfur. Of the 89 proteins predicted to be localized to the outer membrane (OM), two resided on the same contig as, and downstream from, the SoxXYZAB gene cluster (Figure 8). The first of these (OM19) was identified as having homology to (i) β-barrel secretin, general secretion protein GspD, a central component of type II secretion system (T2SS), as well as (ii) the mannose-sensitive hemagglutinin (MSHA)-type pilus assembly protein MshL, a type IV secretion system (T4SS) secretin. The second OM-associated protein (OM20), seven genes downstream from the putative GspD/MshL, was unannotated by Prokka. A BLASTp search for potential homologs identified multiple hits to hypothetical proteins from known SOB, or MAGs from environmental samples where S-oxidation might be an important pathway (Table S5). The nearest hit, at 73.5% ID at 99% query coverage, was a hypothetical protein (WP_124704254.1) from the SOB *Sulfuriferula multivorans*. Alignment of the recovered homologs revealed a conserved proline-cysteine-proline (PCP) motif near the C-terminus of the protein (Figure 9). Phyre2 prediction of protein structure identified Gsp pseudopilin GspG (20% ID, 98.2 confidence) and the type IVa major pilin, PilA (25% ID, 96.4 confidence) as the most appropriate template. Modeled structures and full Phyre2.0 results for OM20 are provided in the supplemental material. Other genes in the gene cluster include a putative AAA family ATPase, a homolog to the inner membrane platform GspF, and several hypothetical proteins unannotated by Prokka. The arrangement of the gene cluster shares remarkable similarity to other T2SS, with the location of several of the small, annotated genes suggesting that they may be type II pseudopilin or type IV pilin subunits. Included in these putative pilin-like subunits is a small protein predicted to be extracellular, located 1 gene downstream from OM20. The best hit from a BLASTp search of this protein was a type II secretion system protein (WP_124704253.1) also from *S. multivorans* with a 73.7% identity and 99% query coverage. The alignment of the putative homologs (Table S6) again returned a conserved PCP as well as a conserved C residue at position 106 (Figure 9).

4 | DISCUSSION

4.1 | Enrichment culture geochemistry and mineralogy

The enhanced generation of sulfate in the presence of a live inoculum under all conditions tested (Figure 2e–h) demonstrates the ability of microorganism from the SSHCZO subsurface to accelerate the oxidation of pyrite in vitro. Microbially enhanced pyrite oxidation was accompanied by scavenging of polythionates, which was otherwise accumulated in abiotic reactors (Figure 2m–p); mechanistic and biogeochemical implication of these results is discussed below. It is important to note that the levels of polythionate accumulation in the abiotic reactors (≤0.097 mM) were ca. 15–62 fold lower than net sulfate release (see Table S7), a result consistent with previous short-term studies of abiotic pyrite oxidation at circumneutral pH (Moses & Herman, 1991). The kinetics of the abiotic reaction of thiosulfate with dissolved oxygen are notoriously slow (Durham, 1974) and our own observations indicate a loss rate of <1% per day in sterile 0.1 mM thiosulfate solutions (data not shown). These findings suggest that rapid turnover of the polythionate pool through abiotic reaction with oxygen was not the major mechanism for sulfate release in the uninoculated reactors. As described below, a key implication of this conclusion is that simple scavenging of polythionates via microbial activity cannot account for the observed stimulation of sulfate release in the biotic reactors.

The pH of cultures that were buffered, either by PIPES, shale, or both, remained largely circumneutral over the course of the experiment (Figure 2a–d). The exception was the shale-free S + Py-B reactors, in which pH decreased to ca. 6 in conjunction with extensive pyrite oxidation (Figure 2a). The S + Py + Sh-UB reactors, which had an initial pH of 7.8, also exhibited biologically accelerated pyrite oxidation (Figure 2h). Together, these results show that this process can occur over a fairly wide range of circumneutral pH. The unbuffered S + Py reactors underwent a precipitous drop in pH over the course of the experiment, and biological enhancement of sulfate generation stopped once the pH reached ca. 4. Concurrent with the decrease in pH were a rapid decrease in ATP (Figure 2j), decline in the abundance of OTUs of the genus *Thiobacillus* (Figure 6), and accumulation of polythionates (Figure 2n). Together, these results suggest cellular death as a result of rapid acidification. Net microbial growth (i.e., increase in ATP) coupled to pyrite oxidation was not observed in any of the other inoculated reactor systems. The simplest explanation for this result is that heterotrophic organisms that had colonized the minerals (see Table S3) in situ declined in biomass when transferred to organics-free SH-AGW. These results preclude direct assessment of whether or not any chemolithoautotrophic growth took place in the inoculated reactors, although genomic evidence (see Section 3.4.2) suggests that such growth could have taken place.

Marked differences were observed in the surface morphology and mineralogy of pyrite from the abiotic versus biotic shale-free reactors (Figure 4). The accumulation of goethite on pyrite surfaces under abiotic conditions is consistent with studies of the naturally weathered pyrites at SSHCZO (Gu, Heaney, et al., 2020), where oxidized pyrite grains show a sequential transition from poorly crystalline Fe oxides to goethite, with goethite more abundant at the outer rim. It is possible that microbially enhanced oxidation of pyrite resulted in a more rapid oxide precipitation, preventing the crystallization to goethite at the pyrite surface (Pichler & Veizer, 1999). Additionally, bacterial cells have been shown to stabilize ferrihydrite, allowing the extended persistence of poorly crystalline phases (Kennedy et al., 2004).

In the presence of shale, both the biotic and abiotic oxidation of pyrite were repressed compared to identical conditions with no shale added (Figure 2e–h). It has previously been reported that the

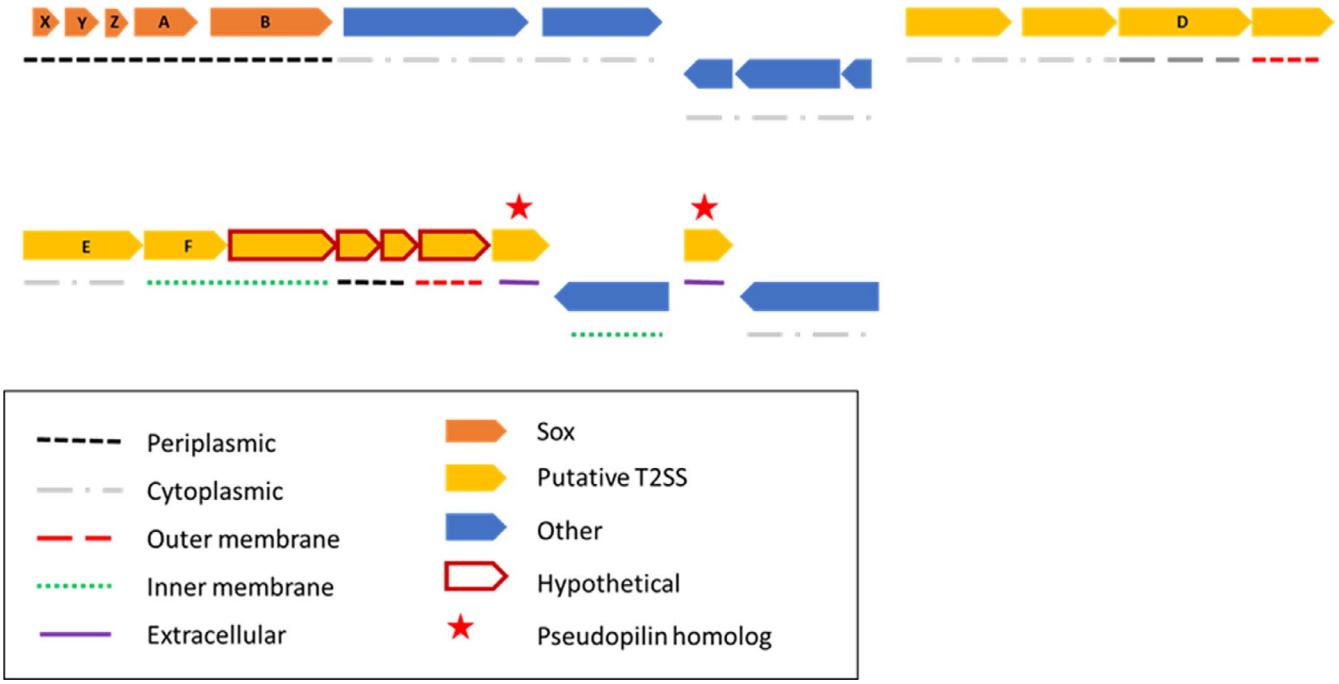

FIGURE 8 Gene map of the Sox gene cluster (orange) from MAG 449, a putative *Thiobacillus* strain illustrating the genomic relationship to a putative T2SS system (Gsp, yellow). Predicted subcellular locations are provided. Hypothetical proteins and putative pseudopilin homologs are indicated

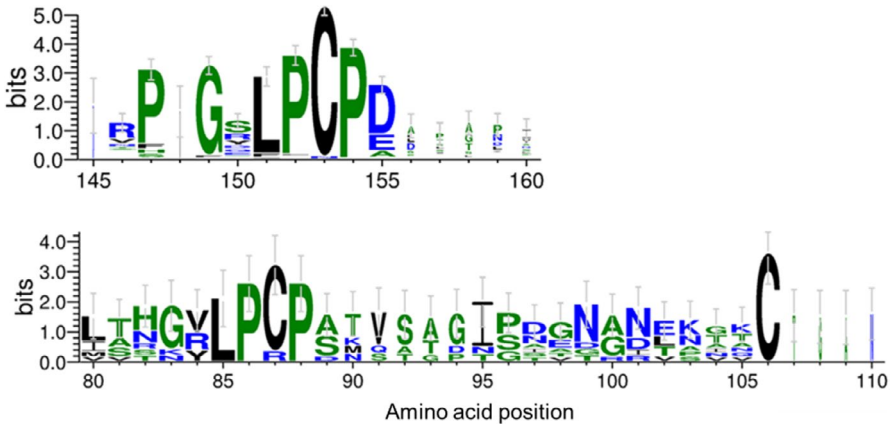

FIGURE 9 Information content (in bits) of amino acid sequence alignments showing location of conserved motifs of the hypothetical sulfhydryl-containing outer membrane protein (top) and the adjacent pseudopilin (bottom) (see Figure 8) and homologs identified by BLASTPp (top) showing conserved regions, including cysteine residues. Stack height is indicative of degree of conservation with error bars representing the 95% confidence interval

formation of a silicate-stabilized passivation layer can greatly inhibit pyrite oxidation (Evangelou, 2001). As shale dissolution was observed across all shale-amended reactors (demonstrated by an increase in Ca and other cation concentrations; Figure 2q–t, Figure S1), it is likely that Si was released to solution during dissolution, and that the lower aqueous Si concentration in pyrite-amended shale reactors (S + Sh + Py) relative to nonpyrite-amended shale reactors (S + Sh) (see Figure S1K–L) is reflective of Si sorption. Si is strongly sorptive to Fe oxyhydroxides at near neutral pH (Swedlund & Webster, 1999), and the lack of goethite crystals in both buffered and unbuffered S + Py + Sh reactors (Figure 5) can be explained by the incorporation of Si into the Fe oxyhydroxide, preventing the further crystallization to crystalline phases such as goethite (Deng, 1997). Similar differences in morphologies between pyrite surface layers were observed during neutral pH (7.4) leaching with and without added Si in solution (Fan et al., 2017). Fan et al. (2017) demonstrated that without Si, pyrite surfaces displayed a needle like structure consistent with goethite; and that when Si was added to solution, Si was associated with an amorphous Fe-oxyhydroxide coating. The amorphous nature of the Si-Fe-oxyhydroxide coating was associated with decreased release of sulfate, a phenomenon attributed to the lower porosity of this layer when compared to layers of discrete goethite crystallites. These observations explain the overall suppression of both biotic and abiotic sulfate release in the presence of shale. When

PIPES was not supplied as a buffer, live, inoculated reactors showed an even further suppression of sulfate release not observed under equivalent abiotic conditions (compare Figure 2g and h). We speculate that this effect could be attributable to a physiological effect related to the elevated pH of the unbuffered reactors (average 7.52) relative to buffered reactors (average (7.23).

4.2 | Metabolic pathways and potential mechanisms for accelerated pyrite oxidation

Metagenome assembled genomes obtained from the pyrite enrichment culture were investigated using metagenomics to gain insight into the potential chemolithotrophic pathways involved in pyrite oxidation. Percak-Dennett et al. (2017) proposed a sorbed Fe redox cycling model for microbially mediated pyrite oxidation, whereby microbial Fe(II) oxidation at the pyrite surface accelerates mineral dissolution. In this model, enzymatic Fe(II) oxidation promotes pyrite oxidation through increased rates of sorbed Fe redox cycling coupled to conduction of electrons to the mineral surface (Moses & Herman, 1991; Percak-Dennett et al., 2017). Metagenomic sequence analysis showed that organisms in the Percak-Dennett et al. (2017) cultures contained extracellular electron transport (EET) pathways postulated to be involved in enzymatic Fe(II) oxidation by neutrophilic FeOB (He et al., 2017). In contrast to those cultures, Fe(II) oxidation does not appear to be the dominant mechanism for acceleration of pyrite oxidation in our experiments. Homologs to either the MtoAB- or Cyc2-based pathways for aerobic Fe(II) oxidation (see He et al., 2017 for review) were found in 14 MAGs obtained from the metagenomic coassembly (Figure 7); however, the relatively low abundance of these MAGs, coupled with the 16S rRNA gene community analysis from days 21 and 77 of the experiment (Figure 6), suggests that their contribution to pyrite oxidation was marginal. If microbially driven sorbed Fe redox cycling were the dominant mechanism, one might expect FeOB to be of higher abundance than SOB, as well as differences to arise in the Fe(II)/Fe(total) ratio between live and control reactors over time, neither of which were observed under our experimental conditions (see Figures 6, 7, and S1). While the low abundances of putative FeOB cannot entirely preclude their potential contribution to enhanced pyrite oxidation, our results nonetheless point to an important role for SOB, in contrast to the work of Percak-Dennett et al. (2017). Based on 16S rRNA gene amplicon analysis of enrichment cultures, the most dominant organisms during times of high pyrite oxidation rates were related to the genus *Thiobacillus*. Two *Thiobacillus*-related MAGs were obtained from the metagenomic coassembly, neither of which contained the well-described MtoABCD- (Beckwith et al., 2015; Liu et al., 2012) or Cyc2 (Castelle et al., 2008; McAllister et al., 2020)-type pathways for EET (see Figure 7). Nevertheless, the possibility remains for an alternative Fe(II) oxidation pathway. For example, a porin-periplasmic multicopper oxidase (MCO) of the PcoA and PcoB protein families has been hypothesized to be involved in chemolithotrophic Fe(II) oxidation (He et al., 2017), and homologs to PcoAB are present in the genome of the two *Thiobacillus* MAGs as well as the genome of *T. denitrificans* ATCC 25259. However, genomic analysis of potential nitrate-dependent Fe(II) oxidation pathways in *T. denitrificans* ATCC 25259 did not indicate the upregulation of a MCO, and a screen of 20,000 random mutants did not yield an Fe(II)-oxidation defective mutant that would suggest a role for MCO (Beller et al., 2013). The PcoAB-type MCO of *T. denitrificans* ATCC 25259 is found within a large gene cluster encoding other genes associated with metal resistance, including two heavy metal efflux systems and an Hg^{2+} resistance system (Beller, Chain, et al., 2006). These results suggest that PcoAB may, in fact, act as a conveyor of copper resistance as opposed to an Fe(II)-oxidation pathway in *T. denitrificans*. Furthermore, while *T. denitrificans* is purported to oxidize nanocrystalline pyrite coupled to nitrate reduction (Bosch et al., 2012), these results were not replicable with purely crystalline pyrite, and it has been suggested that the observed reduction of nitrate resulted from the chemolithotrophic oxidation of reduced sulfur species as impurities in the specimen pyrite or residual S from the initial inocula (Yan et al., 2019). As a caveat, the above-mentioned studies on *T. denitrificans* focus on nitrate-dependent iron or pyrite oxidation, in contrast to this study, where sterile air was supplied to the headspace and the cultures maintained aerobic conditions; however, studies reporting neutral pH aerobic pyrite oxidation are limited making direct comparisons difficult. Together, these findings suggest that Fe(II) oxidation at the pyrite surface by *Thiobacillus* was not responsible for microbially enhanced sulfate release in our experiments.

The presence of the full Sox pathway in putative *Thiobacillus* MAGs is in accordance with the "indirect polythionate intermediate model" proposed by Percak-Dennett et al. (2017). In this model, surface associated SOB scavenge polythionate intermediates (e.g., thiosulfate) released from partial abiotic oxidation of pyrite. The supposition then is that consumption of polythionate intermediates increases the overall reaction rate via Le Chatelier effect. Although SOB have long been recognized to accelerate the oxidation of thiosulfate relative to strictly chemical oxidation (Tuttle & Jannasch, 1976), it is unlikely that Le Chatelier's principle alone can be invoked to explain the enhanced release of sulfate to solution under biotic conditions. This mechanism would assume that the dominant product released from the oxidation of pyrite is polythionates, and that the conversion of polythionates to sulfate is rate limiting. However, as discussed above, both our results and those of Moses and Herman (1991) and Moses et al. (1987) show that sulfate is the primary product of abiotic pyrite oxidation at neutral pH, with the rate of polythionate generation being several-fold lower than sulfate generation. It has been demonstrated that in sterile, dilute thiosulfate solutions, the abiotic rate of thiosulfate reaction with oxygen is relatively slow, remaining stable for years (Durham, 1974). This would suggest that the measured thiosulfate concentrations in the abiotic reactors are a reasonable approximation of the actual thiosulfate generated. In addition, studies with the moderately acidophilic SOB *Thiomonas intermedia*, which has been shown to oxidize intermediate reduced S compounds formed by abiotic FeS_2 oxidation (rather than FeS_2 directly), demonstrated that rates of pyrite oxidation were not affected

by the presence of microbial activity (Arkesteyn, 1980; Schippers et al., 1996). This argument is further supported by thermodynamic calculations, which demonstrate that the free energy of the reaction is unaffected by the concentration of $S_2O_3^{2-}$ (Percak-Dennett et al., 2017). Regardless of whether or not polythionates were produced as intermediates in the biotic reactors, or if scavenging of chemically produced polythionates occurred, our data point to the need for an alternative model by which microorganisms can accelerate sulfate release from pyrite.

The lack of polythionate accumulation in biotic reactors could in fact point to an altogether different mechanism of pyrite oxidation in biotic reactors relative to simple consumption of polythionate intermediates by SOB. One intriguing possibility is the involvement of a dedicated outer membrane protein that interacts directly with the pyrite surface. Intracellularly, S transfer reactions often involve multiple transfers of persulfide moieties between enzymes containing sulfhydryl (thiol) functional groups (e.g., cysteine). Extracellularly, sulfhydryl containing outer membrane proteins (OMPs) have been proposed to mobilize elemental sulfur in acidiphilic S-oxidizing bacteria of the genus *Acidithiobacillus*. The OMP is postulated to form a persulfide bond between a cysteine residue and extracellular sulfur with the sulfane sulfur then serving as the substrate of the periplasmic sulfur dioxygenase (Rohwerder & Sand, 2003). Similar models have been described in *Acidithiobacillus caldus* (Chen et al., 2012; Mangold et al., 2011) and *A. thiooxidans* (Yin et al., 2014). Interestingly, thiol-containing OMPs have also been shown to be differentially expressed in phylogenetically distant mesoacidiphilic to extremely acidiphilic sulfur-oxidizing microorgansims grown on S^0, including the firmicute *Sulfobacillus thermosulfidooxidans* and the Archeon *Acidianus manzaensis* (Liu et al., 2015). While the above studies are restricted to acidophilic taxa, a hypothetical OMP in the neutrophilic ε-proteobacterial SOB *Sulfurimonas denitrificans* was recently shown to be enriched in the proteome when the organism was grown on solid-phase cyclooctasulfur (S_8) compared to thiosulfate (Gotz et al., 2019). While the function of this protein remains unknown, Gotz et al. (2019) identified homologs in other *Campylobacteria* species implicated in the oxidation of elemental sulfur and suggest that it may be involved in the activation of S_8.

While no homologs to the hypothetical protein postulated to be involved in S_8 oxidation were found in the *Thiobacillus* MAGs, the possibility remains of an analogous feature that could mediate direct oxidation of extracellular pyrite S. Although speculative, it is interesting to note the presence of a gene cluster encoding a putative T2SS or T4SS protein secretion systems (see Section 3.4.3) downstream of the Sox operon in the most abundant *Thiobacillus*-related MAG (Figure 8). T2SS are widely distributed among the *Proteobacteria* and employed for a variety of purposes including virulence, adhesion, and nutrient acquisition (Cianciotto, 2005). While most T2SS-secreted proteins are soluble, diffusing away from the cell, T2SS is also known to secrete membrane-anchored proteins (Rondelet & Condemine, 2013) including the lipoproteins MtrC and OmcA used in the respiration of insoluble Fe(III) oxide minerals by *Shewanella oneidensis* (DiChristina et al., 2002; Shi et al., 2008). Rather than for the export of an OM-anchored protein, another possible role of the putative secretory system could be the formation of a pilus-like structure that could interact directly with pyrite surfaces. While T2SS pseudopilins are largely confined to the periplasmic space, it has been shown that they are capable of forming full pilus-like structures extending to the cell surface (Durand et al., 2003; Sauvonnet et al., 2000). Two pseudopilin homologs in the *Thiobacillus* MAG are predicted to be extracellular (Figure 8), in addition to the outer membrane hypothetical protein (OM20), which is predicted to be a pseudopilin based on structural analysis. The putative pseudopilin subunits contain multiple conserved cysteine residues (Figure 9), which could, in theory, be used to transport extracellular persulfide groups to the periplasm for oxidation via the Sox pathway. It remains possible that the conserved cysteine residues common among the putative (pseudo) pilin proteins are of a structural nature, forming C-C disulfide bonds common to true T4SS pilins (Parge et al., 1995). However, protein family (Pfam) alignments of T2SS protein G (PF08334) and TSS2 pseudopilin PulG (PF11773) do not contain any conserved cysteine residues, suggesting their role is not likely to be purely structural if they are, in fact, T2SS pseudopilins. Due to the high degree of similarity between T2SS and T4SS (Peabody et al., 2003) and their overall low similarity to the homologs of these proteins found in the *Thiobacillus* MAGs, it is difficult at this point to infer with certainty which class of secretory systems is constituted by the gene cluster in Figure 8. Regardless, the fact that the nearest BLASTp hits to the above-described putative proteins identified in the *Thiobacillus*-related MAG are SOB is thought-provoking, raising the question of their potential involvement in extracellular pyrite oxidation via a "direct sulfur oxidation" mechanism. A conceptual diagram for the proposed pathway in *Thiobacillus* MAG 449 is provided in Figure 10.

4.3 | Environmental implications

The enhanced generation of sulfate in presence of a live inoculum under all conditions tested (Figure 2e–h) confirms the previously described (Percak-Dennett et al., 2017) ability of microorganisms from subsurface pyrite weathering environments to accelerate aerobic oxidation of pyrite in vitro. The previous study (Percak-Dennett et al., 2017) was conducted with organisms from unconsolidated Miocene-age lacustrine deposits from the Hanford 300 Area site in eastern Washington (Peretyazhko et al., 2012) where geochemical data suggest that oxidation of pyrite is taking place in the vicinity of redox transition zone ca. 18 m below the ground surface (Lin et al., 2012). Although this system differs fundamentally from the hydrogeochemical environment at Shale Hills (see below), the fact that aerobic chemolithotrophic organisms from both environments are able to accelerate pyrite oxidation suggests that such organisms may be common in pyrite-bearing subsurface environments. This idea is supported by recent preliminary studies, which demonstrated the ability of aerobic groundwater microorganisms to accelerate oxidation of native pyrite phases in sandstone aquifer sediments from Wisconsin (Haas et al., 2019).

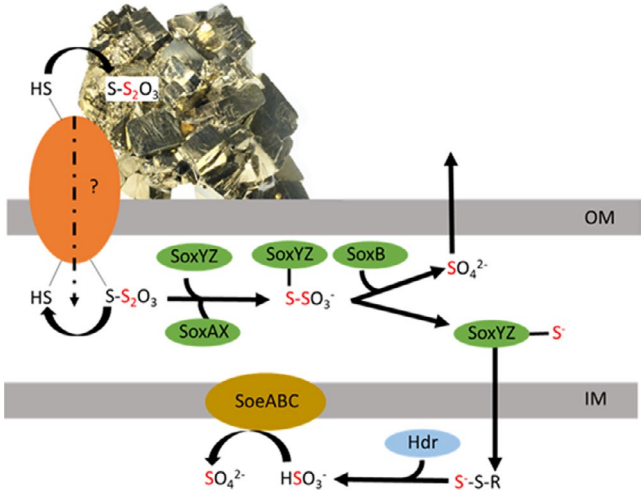

FIGURE 10 Conceptual diagram of the proposed "direct sulfur oxidation" mechanism for microbial circumneutral pyrite oxidation by the putative *Thiobacillus* sp. MAG 449 via the Sox-Hdr-Soe pathway. A putative sulfhydryl-bearing outer membrane (OM) protein (orange, see Figures 8 and 9 for details) mediates the transfer of pyrite sulfur (S) to components of the Sox sulfur oxidation components (green) in the periplasm. Further oxidation of the sulfone sulfur carried by SoxYZ is performed via the cytoplasmic heterodisulfide reductase (Hdr, blue) and the inner membrane bound sulfite oxidation enzyme (SoeABC, mustard)

It is important to consider the physical and geological characteristics of subsurface environments when evaluating what role chemolithotrophs may play in the oxidation of reduced Fe and S minerals in natural systems. To illustrate this idea, consider the subsurface oxidative weathering of Fe(II)-silicate minerals in granitic bedrock (Rio Blanco Quartz Diorite) from the Luquillo Critical Zone Observatory in Puerto Rico. In this system, chemolithotrophic FeOB resides in partially altered, fractured, rocky material termed the "rindlet zone" (Turner et al., 2003), where direct contact with mineral surfaces is feasible (Buss et al., 2005; Minyard et al., 2012). In the outer rindlet zone, the weathering of the Fe(II)-silicate mineral hornblende is rapid, becoming completely depleted over a scale of centimeters (Buss et al., 2005, 2008). We recently demonstrated in laboratory experiments that chemolithotrophic FeOB can mediate the oxidation of the Fe(II)-silicate minerals biotite and hornblende in the Rio Blanco Quartz Diorite at substantial rates compared to zero rates of reaction under abiotic conditions (Napieralski et al., 2019; Napieralski & Roden, 2020). Although translation of the laboratory results to in situ weathering rates is not yet possible, the presence of fractures and the existence of relatively fine-grained granitic fragments within the rindlet zone strongly suggest that microorganisms are likely to play a role in oxidative Fe(II)-silicate weathering. Similar conclusions were reached by Percak-Dennett et al. (2017) regarding the likely participation of chemolithotrophic microorganisms in pyrite oxidation within the redox transition zone at the Hanford 300 Area site.

In contrast to the Hanford 300 Area redox transition zone and Luquillo rindlet zone environments, oxidation of pyrite in the Rose Hill Shale at the SSHCZO occurs at a depth where very little significant disaggregation of the nanoporous protolith is observed (Brantley et al., 2013; Gu, Heaney, et al., 2020). Thus, direct contact of microbial cells with pyrite is without question limited by the nanoporosity of the Rose Hill Shale, with the potential exception of pyrite exposed on fracture surfaces (see illustration in Figure 1). In light of this reality, Gu, Heaney, et al. (2020) argued that it seems unlikely that any direct contact mechanism can be a large contributor to oxidative weathering of pyrite at SSHCZO. This precludes, therefore, either the previously proposed sorbed Fe redox cycling mechanism, or the newly proposed direct sulfur oxidation pathway. In addition, in stark contrast to the total lack of abiotic Fe(II)-silicate oxidation after ca. 2.4 years of abiotic incubation reported by Napieralski et al. (2019), our experiments show that significant pyrite oxidation proceeds under long-term abiotic incubation. As evidenced by the careful analytical work of Gu, Heaney, et al. (2020), S is completely depleted during in situ pyrite weathering at the grain scale within the nanoporous matrix at SSHCZO. The lack of observable S phases on the oxidized pyrite indicates complete S removal and suggests that diffusion of thiosulfate (or sulfate) is not limiting with regard to in situ oxidation. Hence, scavenging of polythionates via the "polythionate intermediate model" is also unlikely to lead to accelerated pyrite oxidation in situ. This assertion is in accordance with our experimental findings that thiosulfate consumption by SOB is unlikely to significantly accelerate pyrite oxidation in vitro (see Section 4.1). It thus seems unlikely that either FeOB or SOB can effectively accelerate pyrite oxidation at a large scale in the Rose Hill shale. In particular, as suggested by Gu, Heaney, et al. (2020), under most of the catchment, pyrite oxidation is occurring in the shale where nanopores are too small to allow access by micro-organisms, and so oxidation is likely to be abiotic. However, Gu, Heaney, et al. (2020) also suggested that biotic oxidation could be occurring along fracture walls where micro-organisms can gain access, or possibly under the valley of the Shale Hills watersheds where pore sizes are sometimes observed to be large even at depths near the pyrite oxidation front. Thus, on some fracture walls and under the valley where pyrite oxidation is thought to dictate the pace of incision, it is possible that microbial enhancement may occur.

Despite the assertion that pyrite oxidation at SSHCZO must largely proceed abiotically, this work provides new insight into the potential mechanisms by which microorganisms may accelerate pyrite oxidation at circumneutral pH. In circumneutral environments where the geological setting is appropriate to allow for direct microbial colonization of mineral surfaces, it is conceivable that microbially mediated pyrite oxidation may be an important, perhaps dominant, biogeochemical process. Studies in a wide range of such pyrite-oxidizing environments have noted an abundance of organisms of the genus *Thiobacillus*, suggestive of a common functionality for this ubiquitous taxon. Investigations of black shale weathering have identified *Thiobacillus* related 16S rRNA gene sequences in an in situ incubation experiment (Zhu & Reinfelder, 2012) and in a study investigating black shale weathering profile developed near a roadcut in southwest China (Li et al., 2014). Additionally, it has been reported

that pyrite exerts a strong mineralogical control on microbial community structure in subglacial environments (Mitchell et al., 2013) and lithoautotrophic oxidation of sulfide minerals in such environments, including by *Thiobacillus* (Harrold et al., 2015), is postulated to be a driver of subglacial primary productivity and mineral weathering (Boyd et al., 2014; Montross et al., 2013; Skidmore et al., 2005). Rapid exposure of fresh pyrite in recent landslides (Emberson et al., 2016) could also produce a habitat capable of supporting chemolithotrophic circumneutral pH pyrite oxidation activity. Similarly, microbial circumneutral pyrite oxidation is likely to be of importance in the early stages of AMD generation where mining activity exposes fresh mineral surfaces for microbial colonization prior to the onset of rapid acidification. Investigations of mine tailings have shown that pH is an important driver of microbial community structure (Chen et al., 2013, 2014) and *Thiobacillus* seems to be an important community member in mining waste (Blowes et al., 2003; Korehi et al., 2014; Liu et al., 2014; Schippers et al., 2010).

5 | CONCLUSIONS

Pyrite-oxidizing enrichment cultures established using an inoculum from a natural subsurface pyrite weathering system demonstrated enhanced sulfate generation relative to uninoculated controls under circumneutral pH conditions. Whether artificially buffered with PIPES or naturally buffered by the native shale, rapid acidification of the bulk culture media was prevented despite extensive pyrite oxidation, resulting in long-term circumneutral pH conditions where organisms of the genus *Thiobacillus* dominated enrichment cultures. Metagenomic analysis revealed that the dominant chemolithotrophic pathway in enrichment cultures was oxidation of reduced S. The most abundant chemolithotrophic MAG, a putative *Thiobacillus* species, contained a full reduced S oxidation pathway. Scavenging of polythionate intermediates is insufficient to explain the enhanced generation of sulfate from pyrite in the presence of SOB. We thus propose a new "direct sulfur oxidation" pathway to explain this phenomenon. While we conclude that the sorbed Fe redox model proposed by Percak-Dennett et al. (2017) is not likely to be the dominant mechanism of accelerated pyrite oxidation in our enrichment cultures, it can by no means be discounted as a potential pathway in all systems. The possibility remains that FeOB are capable of accelerating the circumneutral oxidation of pyrite and that our enrichment in SOB is unique to this study. In the context of subsurface shale weathering, the oxidation of pyrite in the Rose Hill Shale at SSHCZO largely proceeds abiotically, as physical contact between mineral surfaces and living cells, which is almost certainly required for biotic catalysis (either by the sorbed Fe redox cycling or the direct sulfur oxidation pathway), is likely not possible in the nanoporous shale matrix. Only in certain locations, such as under the valley of the watershed, it is possible for pores to be large enough for microbial enhancement of weathering. Thus, our understanding of microbial chemolithotrophic oxidation of pyrite at circumneutral pH is still in its infancy, and further studies in the types of environments likely to be conducive to the process are needed to gain a fuller understanding of mechanistic underpinnings and biogeochemical significance of this as yet poorly documented phenomenon.

ACKNOWLEDGMENTS

The field research was conducted in Penn State's Stone Valley Forest, which is funded by the Penn State College of Agriculture Sciences, Department of Ecosystem Science and Management, and managed by the staff of the Forestlands Management Office. Financial Support for the field site and Brandon Forsythe was provided by National Science Foundation Grants EAR-1239285 (SLB) and EAR-1331726 (SLB) for the Susquehanna Shale Hills Critical Zone Observatory. Laboratory work and DNA sequencing were supported by the NASA Astrobiology Institute and a University of Wisconsin Microbiome Initiative award to EER. We also would like to thank Dr. Xin Gu for his helpful discussions.

DATA AVAILABILITY STATEMENT

TDNA sequencing data that support the findings of this study have been deposited in The National Center for Biotechnology Information (https://www.ncbi.nlm.nih.gov/) under the BioProject Number PRJNA692452. Addition data not found in the supplementary material of this article are available are available from the corresponding author upon reasonable request.

ORCID

Stephanie A. Napieralski https://orcid.org/0000-0001-5887-2096
Yihang Fang https://orcid.org/0000-0002-8218-5883
Eric E. Roden https://orcid.org/0000-0002-1555-4343

REFERENCES

Alneberg, J., Bjarnason, B. S., de Bruijn, I., Schirmer, M., Quick, J., Ijaz, U. Z., Lahti, L., Loman, N. J., Andersson, A. F., & Quince, C. (2014). Binning metagenomic contigs by coverage and composition. *Nature Methods*, *11*(11), 1144–1146. https://doi.org/10.1038/nmeth.3103

Altschul, S. F., Gish, W., Miller, W., Myers, E. W., & Lipman, D. J. (1990). Basic local alignment search tool. *Journal of Molecular Biology*, *215*(3), 403–410. https://doi.org/10.1016/S0022-2836(05)80360-2

Amiotte Suchet, P., Probst, J.-L., & Ludwig, W. (2003). Worldwide distribution of continental rock lithology: Implications for the atmospheric/soil CO_2 uptake by continental weathering and alkalinity river transport to the oceans. *Global Biogeochemical Cycles*, *17*(2), 1038. https://doi.org/10.1029/2002GB001891

Appia-Ayme, C., Guiliani, N., Ratouchniak, J., & Bonnefoy, V. (1999). Characterization of an operon encoding two c-type cytochromes an aa3-type cytochrome oxidase, and rusticyanin in *Acidithiobcillus ferrooxidans* ATCC 33020. *Applied and Environmental Microbiology*, *65*(11), 4781–4787.

Arkesteyn, G. J. M. W. (1980). Pyrite oxidation in acid sulphate soils: The role of miroorganisms. *Plant and Soil*, *54*(1), 119–134. https://doi.org/10.1007/BF02182004

Aronesty, E. (2013). Comparison of sequencing utility programs. *The Open Bioinformatics Journal*, *7*, 1–8. https://doi.org/10.2174/1875036201307010001

Baker, B. J., & Banfield, J. F. (2003). Microbial communities in acid mine drainage. *FEMS Microbiology Ecology*, *44*(2), 139–152. https://doi.org/10.1016/S0168-6496(03)00028-X

Beckwith, C. R., Edwards, M. J., Lawes, M., Shi, L., Butt, J. N., Richardson, D. J., & Clarke, T. A. (2015). Characterization of MtoD from *Sideroxydans lithotrophicus*: A cytochrome c electron shuttle used in lithoautotrophic growth. *Frontiers in Microbiology*, *6*, 332. https://doi.org/10.3389/fmicb.2015.00332

Beller, H. R., Chain, P. S. G., Letain, T. E., Chakicherla, A., Larimer, F. W., Richardson, P. M., Coleman, M. A., Wood, A. P., & Kelly, D. P. (2006). The genome sequence of the obligately chemolithoautotrophic, facultatively anaerobic bacterium *Thiobacillus denitrificans*. *Journal of Bacteriology*, *188*(4), 1473–1488.

Beller, H. R., Letain, T. E., Chakicherla, A., Kane, S. R., Legler, T. C., & Coleman, M. A. (2006). Whole-genome transcriptional analysis of chemolithoautotrophic thiosulfate oxidation by *Thiobacillus denitrificans* under aerobic versus denitrifying conditions. *Journal of Bacteriology*, *188*(19), 7005–7015.

Beller, H. R., Zhou, P., Legler, T. C., Chakicherla, A., Kane, S., Letain, T. E., & A. O'Day, P. (2013). Genome-enabled studies of anaerobic, nitrate-dependent iron oxidation in the chemolithoautotrophic bacterium *Thiobacillus denitrificans*. *Frontiers in Microbiology*, *4*, 249. https://doi.org/10.3389/fmicb.2013.00249

Berner, R. A. (1984). Sedimentary pyrite formation: An update. *Geochimica Et Cosmochimica Acta*, *48*(4), 605–615. https://doi.org/10.1016/0016-7037(84)90089-9

Berner, R. A. (2006). GEOCARBSULF: A combined model for Phanerozoic atmospheric O2 and CO2. *Geochimica Et Cosmochimica Acta*, *70*(23), 5653–5664. https://doi.org/10.1016/j.gca.2005.11.032

Blowes, D. W., Ptacek, C. J., Jambor, J. L., & Weisener, C. G. (2003). The geochemistry of acid mine drainage. *Treatise on Geochemistry*, *9*, 149–204.

Bolton, E. W., Berner, R. A., & Petsch, S. T. (2006). The weathering of sedimentary organic matter as a control on atmospheric O2: II. Theoretical modeling. *American Journal of Science*, *306*(8), 575–615. https://doi.org/10.2475/08.2006.01

Bosch, J., Lee, K. Y., Jordan, G., Kim, K. W., & Meckenstock, R. U. (2012). Anaerobic, nitrate-dependent oxidation of pyrite nanoparticles by *Thiobacillus denitrificans*. *Environmental Science and Technology*, *46*(4), 2095–2101.

Bosch, J., & Meckenstock, R. U. (2012). Rates and potential mechanism of anaerobic nitrate-dependent microbial pyrite oxidation. *Biochemical Society Transactions*, *40*(6), 1280–1283. https://doi.org/10.1042/BST20120102

Boyd, E. S., Hamilton, T. L., Havig, J. R., Skidmore, M. L., & Shock, E. L. (2014). Chemolithotrophic primary production in a subglacial ecosystem. *Applied and Environment Microbiology*, *80*(19), 6146–6153. https://doi.org/10.1128/AEM.01956-14

Brantley, S. L., Holleran, M. E., Jin, L., & Bazilevskaya, E. (2013). Probing deep weathering in the Shale Hills Critical Zone Observatory, Pennsylvania (USA): The hypothesis of nested chemical reaction fronts in the subsurface. *Earth Surface Processes and Landforms*, *38*(11), 1280–1298. https://doi.org/10.1002/esp.3415

Brantley, S. L., White, T., West, N., Williams, J. Z., Forsythe, B., Shapich, D., Kaye, J., Lin, H., Shi, Y., Kaye, M., Herndon, E., Davis, K. J., He, Y., Eissenstat, D., Weitzman, J., DiBiase, R., Li, L. I., Reed, W., Brubaker, K., & Gu, X. (2018). Susquehanna shale hills critical zone observatory: Shale hills in the context of shaver's creek watershed. *Vadose Zone Journal*, *17*(1), 1–19. https://doi.org/10.2136/vzj2018.04.0092

Buss, H. L., Bruns, M. A., Schultz, M. J., Moore, J., Mathur, C. F., & Brantley, S. L. (2005). The coupling of biological iron cycling and mineral weathering during saprolite formation, Luquillo Mountains, Puerto Rico. *Geobiology*, *3*, 247–260. https://doi.org/10.1111/j.1472-4669.2006.00058.x

Buss, H. L., Sak, P. B., Webb, S. M., & Brantley, S. L. (2008). Weathering of the Rio Blanco quartz diorite, Luquillo Mountains, Puerto Rico: Coupling oxidation, dissolution, and fracturing. *Geochimica Et Cosmochimica Acta*, *72*(18), 4488–4507. https://doi.org/10.1016/j.gca.2008.06.020

Caporaso, J. G., Bittinger, K., Bushman, F. D., DeSantis, T. Z., Andersen, G. L., & Knight, R. (2010). PyNAST: A flexible tool for aligning sequences to a template alignment. *Bioinformatics*, *26*(2), 266–267. https://doi.org/10.1093/bioinformatics/btp636

Caporaso, J. G., Kuczynski, J., Stombaugh, J., Bittinger, K., Bushman, F. D., Costello, E. K., Fierer, N., Peña, A. G., Goodrich, J. K., Gordon, J. I., Huttley, G. A., Kelley, S. T., Knights, D., Koenig, J. E., Ley, R. E., Lozupone, C. A., McDonald, D., Muegge, B. D., Pirrung, M., … Knight, R. (2010). QIIME allows analysis of high-throughput community sequencing data. *Nature Methods*, *7*(5), 335–336. https://doi.org/10.1038/nmeth.f.303

Castelle, C., Guiral, M., Malarte, G., Ledgham, F., Leroy, G., Brugna, M., & Giudici-Orticoni, M.-T. (2008). A new iron-oxidizing/O2-reducing supercomplex spanning both inner and outer membranes, isolated from the extreme acidophile *Acidithiobacillus ferrooxidans*. *Journal of Biological Chemistry*, *283*(38), 25803–25811. https://doi.org/10.1074/jbc.M802496200

Chen, L.-X., Li, J.-T., Chen, Y.-T., Huang, L.-N., Hua, Z.-S., Hu, M., & Shu, W.-S. (2013). Shifts in microbial community composition and function in the acidification of a lead/zinc mine tailings. *Environmental Microbiology*, *15*(9), 2431–2444. https://doi.org/10.1111/1462-2920.12114

Chen, L., Ren, Y., Lin, J., Liu, X., Pang, X., & Lin, J. (2012). *Acidithiobacillus caldus* sulfur oxidation model based on transcriptome analysis between the wild type and sulfur oxygenase reductase defective mutant. *PLoS One*, *7*(9), e39470. https://doi.org/10.1371/journal.pone.0039470

Chen, Y.-T., Li, J.-T., Chen, L.-X., Hua, Z.-S., Huang, L.-N., Liu, J., Xu, B.-B., Liao, B., & Shu, W.-S. (2014). Biogeochemical processes governing natural pyrite oxidation and release of acid metalliferous drainage. *Environmental Science and Technology*, *48*(10), 5537–5545. https://doi.org/10.1021/es500154z

Cianciotto, N. P. (2005). Type II secretion: A protein secretion system for all seasons. *Trends in Microbiology*, *13*(12), 581–588. https://doi.org/10.1016/j.tim.2005.09.005

Clesceri, L. S., Greenberg, A. E., & Eaton, A. D. (1998). *Standard methods for the examination of water and wastewater* (pp. 4–415). American Public Health Association.

Cockell, C. S., Pybus, D., Olsson-Francis, K., Kelly, L., Petley, D., Rosser, N., Howard, K., & Mosselmans, F. (2011). Molecular characterization and geological microenvironment of a microbial community inhabiting weathered receding shale cliffs. *Microbial Ecology*, *61*(1), 166–181. https://doi.org/10.1007/s00248-010-9730-6

Colmer, A. R., & Hinkle, M. E. (1947). The role of microorganisms in acid mine drainage: A preliminary report. *Science*, *106*(2751), 253–256. https://doi.org/10.1126/science.106.2751.253

Converse, B. J., McKinley, J. P., Resch, C. T., & Roden, E. E. (2015). Microbial mineral colonization across a subsurface redox transition zone. *Frontiers in Microbiology*, *6*, 858. https://doi.org/10.3389/fmicb.2015.00858

Crooks, G. E., Hon, G., Chandonia, J. M., & Brenner, S. E. (2004). WebLogo: A sequence logo generator. *Genome Research*, *14*(6), 1188–1190. https://doi.org/10.1101/gr.849004

Dahl, C., Engels, S., Pott-Sperling, A. S., Schulte, A., Sander, J., Lübbe, Y., Deuster, O., & Brune, D. C. (2005). Novel genes of the dsr gene cluster and evidence for close interaction of Dsr proteins during sulfur oxidation in the phototrophic sulfur bacterium *Allochromatium vinosum*. *Journal of Bacteriology*, *187*(4), 1392–1404.

Dahl, C., Franz, B., Hensen, D., Kesselheim, A., & Zigann, R. (2013). Sulfite oxidation in the purple sulfur bacterium *Allochromatium vinosum*: Identification of SoeABC as a major player and relevance of SoxYZ in the process. *Microbiology*, *159*(Pt 12), 2626–2638. https://doi.org/10.1099/mic.0.071019-0

Deng, Y. (1997). Formation of iron(III) hydroxides from homogeneous solutions. *Water Research*, *31*(6), 1347–1354. https://doi.org/10.1016/S0043-1354(96)00388-0

DiChristina, T. J., Moore, C. M., & Haller, C. A. (2002). Dissimilatory Fe(III) and Mn(IV) reduction by *Shewanella putrefaciens* requires ferE, a homolog of the pulE (gspE) type II protein secretion gene. *Journal of Bacteriology*, *184*(1), 142–151.

Durand, E., Bernadac, A., Ball, G., Lazdunski, A., Sturgis, J. N., & Filloux, A. (2003). Type II protein secretion in *Pseudomonas aeruginosa*: The pseudopilus is a multifibrillar and adhesive structure. *Journal of Bacteriology*, *185*(9), 2749–2758.

Durham, B. W. (1974). Stability of weak sodium thiosulfate solutions. *Analytical Chemistry*, *46*(14), 2245. https://doi.org/10.1021/ac60350a032

Edgar, R. C. (2004). MUSCLE: Multiple sequence alignment with high accuracy and high throughput. *Nucleic Acids Research*, *32*(5), 1792–1797. https://doi.org/10.1093/nar/gkh340

Edgar, R. C. (2010). Search and clustering orders of magnitude faster than BLAST. *Bioinformatics*, *26*(19), 2460–2461. https://doi.org/10.1093/bioinformatics/btq461

Edwards, K. J., Rogers, D. R., Wirsen, C. O., & McCollom, T. M. (2003). Isolation and characterization of novel psychrophilic, neutrophilic, fe-oxidizing, chemolithoautotrophic - and -proteobacteria from the deep sea. *Applied and Environmental Microbiology*, *69*(5), 2906–2913.

Emberson, R., Hovius, N., Galy, A., & Marc, O. (2016). Oxidation of sulfides and rapid weathering in recent landslides. *Earth Surface Dynamics*, *4*(3), 727–742. https://doi.org/10.5194/esurf-4-727-2016

Emerson, D., Field, E. K., Chertkov, O., Davenport, K. W., Goodwin, L., Munk, C., Nolan, M., & Woyke, T. (2013). Comparative genomics of freshwater Fe-oxidizing bacteria: Implications for physiology, ecology, and systematics. *Frontiers in Microbiology*, *4*, 254. https://doi.org/10.3389/fmicb.2013.00254

Emerson, D., Fleming, E. J., & McBeth, J. M. (2010). Iron-oxidizing bacteria: An environmental and genomic perspective. *Annual Review of Microbiology*, *64*, 561–583. https://doi.org/10.1146/annurev.micro.112408.134208

Evangelou, V. P. (2001). Pyrite microencapsulation technologies: Principles and potential field application. *Ecological Engineering*, *17*(2–3), 165–178. https://doi.org/10.1016/S0925-8574(00)00156-7

Fan, R., Short, M. D., Zeng, S.-J., Qian, G., Li, J., Schumann, R. C., Kawashima, N., Smart, R. S. C., & Gerson, A. R. (2017). The formation of silicate-stabilized passivating layers on pyrite for reduced acid rock drainage. *Environmental Science and Technology*, *51*(19), 11317–11325. https://doi.org/10.1021/acs.est.7b03232

Friedrich, C. G., Rother, D., Bardischewsky, F., Quentmeier, A., & Fischer, J. (2001). Oxidation of reduced inorganic sulfur compounds by bacteria: Emergence of a common mechanism? *Applied and Environment Microbiology*, *67*(7), 2873–2882. https://doi.org/10.1128/AEM.67.7.2873-2882.2001

Gotz, F., Pjevac, P., Markert, S., McNichol, J., Becher, D., Schweder, T., Mussmann, M., & Sievert, S. M. (2019). Transcriptomic and proteomic insight into the mechanism of cyclooctasulfur- versus thiosulfate-oxidation by the chemolithoautotroph *Sulfurimonas denitrificans*. *Environmental Microbiology*, *21*(1), 244–258.

Gu, X., Heaney, P. J., Reis, F. D. A. A., & Brantley, S. L. (2020). Deep abiotic weathering of pyrite. *Science*, *370*(6515), eabb8092. https://doi.org/10.1126/science.abb8092

Gu, X., Mavko, G., Ma, L., Oakley, D., Accardo, N., Carr, B. J., Nyblade, A. A., & Brantley, S. L. (2020). Seismic refraction tracks porosity generation and possible CO2 production at depth under a headwater catchment. *Proceedings of the National Academy of Sciences of the United States of America*, *117*(32), 18991–18997.

Guindon, S., Dufayard, J.-F., Lefort, V., Anisimova, M., Hordijk, W., & Gascuel, O. (2010). New algorithms and methods to estimate maximum-likelihood phylogenies: assessing the performance of PhyML 3.0. *Systematic Biology*, *59*(3), 307–321. https://doi.org/10.1093/sysbio/syq010

Haaijer, S. C. M., Lamers, L. P. M., Smolders, A. J. P., Jetten, M. S. M., & Op den Camp, H. J. M. (2007). Iron sulfide and pyrite as potential electron donors for microbial nitrate reduction in freshwater wetlands. *Geomicrobiology Journal*, *24*(5), 391–401. https://doi.org/10.1080/01490450701436489

Haas, L. D., Roden, E. E., Ginder-Vogel, M., & Zambito, J. J. (2019). Microbially-mediated pyrite oxidation at circumneutral pH in sandstones of Trempealeau County, WI. In *Annual Meeting. Abstract 104-8*. Geological Society of America.

Harrold, Z. R., Skidmore, M. L., Hamilton, T. L., Desch, L., Amada, K., van Gelder, W., Glover, K., Roden, E. E., & Boyd, E. S. (2015). Aerobic and anaerobic thiosulfate oxidation by a cold-adapted, subglacial chemoautotroph. *Applied and Environmental Microbiology*, *82*(5), 1486–1495. https://doi.org/10.1128/AEM.03398-15

He, S., Barco, R. A., Emerson, D., & Roden, E. E. (2017). Comparative genomic analysis of neutrophilic iron(II) oxidizer genomes for candidate genes in extracellular electron transfer. *Frontiers in Microbiology*, *8*, 1584. https://doi.org/10.3389/fmicb.2017.01584

Hyatt, D., Chen, G.-L., LoCascio, P. F., Land, M. L., Larimer, F. W., & Hauser, L. J. (2010). Prodigal: Prokaryotic gene recognition and translation initiation site identification. *BMC Bioinformatics*, *11*, 119. https://doi.org/10.1186/1471-2105-11-119

Jin, L., Ogrinc, N., Yesavage, T., Hasenmueller, E. A., Ma, L., Sullivan, P. L., Kaye, J., Duffy, C., & Brantley, S. L. (2014). The CO 2 consumption potential during gray shale weathering: Insights from the evolution of carbon isotopes in the Susquehanna Shale Hills critical zone observatory. *Geochimica Et Cosmochimica Acta*, *142*, 260–280. https://doi.org/10.1016/j.gca.2014.07.006

Jin, L., Ravella, R., Ketchum, B., Bierman, P. R., Heaney, P., White, T., & Brantley, S. L. (2010). Mineral weathering and elemental transport during hillslope evolution at the Susquehanna/Shale Hills Critical Zone Observatory. *Geochimica Et Cosmochimica Acta*, *74*(13), 3669–3691. https://doi.org/10.1016/j.gca.2010.03.036

Jin, L., Rother, G., Cole, D. R., Mildner, D. F. R., Duffy, C. J., & Brantley, S. L. (2011). Characterization of deep weathering and nanoporosity development in shale–A neutron study. *American Mineralogist*, *96*(4), 498–512. https://doi.org/10.2138/am.2011.3598

Jørgensen, C. J., Jacobsen, O. S., Elberling, B., & Aamand, J. (2009). Microbial oxidation of pyrite coupled to nitrate reduction in anoxic groundwater sediment. *Environmental Science & Technology*, *43*(13), 4851–4857. https://doi.org/10.1021/es803417s

Kang, D. D., Li, F., Kirton, E., Thomas, A., Egan, R., An, H., & Wang, Z. (2019). MetaBAT 2: An adaptive binning algorithm for robust and efficient genome reconstruction from metagenome assemblies. *PeerJ*, *7*, e7359. https://doi.org/10.7717/peerj.7359

Kelley, L. A., Mezulis, S., Yates, C. M., Wass, M. N., & Sternberg, M. J. E. (2015). The Phyre2 web portal for protein modeling, prediction and analysis. *Nature Protocols*, *10*(6), 845–858. https://doi.org/10.1038/nprot.2015.053

Kennedy, C. B., Scott, S. D., & Ferris, F. G. (2004). Hydrothermal phase stabilization of 2-line ferrihydrite by bacteria. *Chemical Geology*, *212*(3–4), 269–277. https://doi.org/10.1016/j.chemgeo.2004.08.017

Koch, T., & Dahl, C. (2018). A novel bacterial sulfur oxidation pathway provides a new link between the cycles of organic and inorganic sulfur compounds. *ISME Journal*, *12*(10), 2479–2491. https://doi.org/10.1038/s41396-018-0209-7

Korehi, H., Blothe, M., & Schippers, A. (2014). Microbial diversity at the moderate acidic stage in three different sulfidic mine tailings dumps generating acid mine drainage. *Research in Microbiology*, *165*(9), 713–718. https://doi.org/10.1016/j.resmic.2014.08.007

Le, S. Q., & Gascuel, O. (2008). An improved general amino acid replacement matrix. *Molecular Biology and Evolution*, *25*(7), 1307–1320. https://doi.org/10.1093/molbev/msn067

Li, D., Liu, C. M., Luo, R., Sadakane, K., & Lam, T. W. (2015). MEGAHIT: an ultra-fast single-node solution for large and complex metagenomics

assembly via succinct de Bruijn graph. *Bioinformatics*, *31*(10), 1674–1676. https://doi.org/10.1093/bioinformatics/btv033

Li, J., Sun, W., Wang, S., Sun, Z., Lin, S., & Peng, X. (2014). Bacteria diversity, distribution and insight into their role in S and Fe biogeochemical cycling during black shale weathering. *Environmental Microbiology*, *16*(11), 3533–3547. https://doi.org/10.1111/1462-2920.12536

Lin, X., Kennedy, D., Peacock, A., McKinley, J., Resch, C. T., Fredrickson, J., & Konopka, A. (2012). Distribution of microbial biomass and potential for anaerobic respiration in Hanford site 300 area subsurface sediment. *Applied and Environmental Microbiology*, *78*(3), 759–767. https://doi.org/10.1128/AEM.07404-11

Littke, R., Klussmann, U., Krooss, B., & Leythaeuser, D. (1991). Quantification of loss of calcite, pyrite, and organic matter due to weathering of Toarcian black shales and effects on kerogen and bitumen characteristics. *Geochimica Et Cosmochimica Acta*, *55*(11), 3369–3378. https://doi.org/10.1016/0016-7037(91)90494-P

Liu, H. C., Xia, J. L., Nie, Z. Y., Zhen, X. J., & Zhang, L. J. (2015). Differential expression of extracellular thiol groups of moderately thermophilic *Sulfobacillus thermosulfidooxidans* and extremely thermophilic *Acidianus manzaensis* grown on S(0) and Fe (2.). *Archives of Microbiology*, *197*(6), 823–831. https://doi.org/10.1007/s00203-015-1111-6

Liu, J., Hua, Z.-S., Chen, L.-X., Kuang, J.-L., Li, S.-J., Shu, W.-S., & Huang, L.-N. (2014). Correlating microbial diversity patterns with geochemistry in an extreme and heterogeneous environment of mine tailings. *Applied and Environment Microbiology*, *80*(12), 3677–3686. https://doi.org/10.1128/AEM.00294-14

Liu, J., Wang, Z., Belchik, S. M., Edwards, M. J., Liu, C., Kennedy, D. W., Merkley, E. D., Lipton, M. S., Butt, J. N., Richardson, D. J., Zachara, J. M., Fredrickson, J. K., Rosso, K. M., & Shi, L. (2012). Identification and characterization of MtoA: A decaheme c-type cytochrome of the neutrophilic Fe(II)-oxidizing bacterium *Sideroxydans lithotrophicus* ES-1. *Frontiers in Microbiology*, *3*, 37. https://doi.org/10.3389/fmicb.2012.00037

Ma, L., Chabaux, F., West, N., Kirby, E., Jin, L., & Brantley, S. (2013). Regolith production and transport in the Susquehanna Shale Hills Critical Zone Observatory, Part 1: Insights from U-series isotopes. *Journal of Geophysical Research: Earth Surface*, *118*(2), 722–740. https://doi.org/10.1002/jgrf.20037

Ma, L., Jin, L., & Brantley, S. L. (2011). Geochemical behaviors of different element groups during shale weathering at the Susquehanna/Shale Hills Critical Zone Observatory. *Applied Geochemistry*, *26*, S89–S93. https://doi.org/10.1016/j.apgeochem.2011.03.038

Mangold, S., Valdes, J., Holmes, D. S., & Dopson, M. (2011). Sulfur metabolism in the extreme acidophile *Acidithiobacillus caldus*. *Frontiers in Microbiology*, *2*, 17. https://doi.org/10.3389/fmicb.2011.00017

McAllister, S. M., Polson, S. W., Butterfield, D. A., Glazer, B. T., Sylvan, J. B., & Chan, C. S. (2020). Validating the Cyc2 neutrophilic iron oxidation pathway using meta-omics of *Zetaproteobacteria* iron mats at marine hydrothermal vents. *mSystems*, *5*(1). https://doi.org/10.1128/mSystems.00553-19

McKibben, M. A., & Barnes, H. L. (1986). Oxidation of pyrite in low temperature acidic solutions: Rate laws and surface textures. *Geochimica Et Cosmochimica Acta*, *50*(7), 1509–1520. https://doi.org/10.1016/0016-7037(86)90325-X

Minyard, M. L., Bruns, M. A., Liermann, L. J., Buss, H. L., & Brantley, S. L. (2012). Bacterial associations with weathering minerals at the regolith-bedrock interface, Luquillo experimental forest, Puerto Rico. *Geomicrobiology Journal*, *29*(9), 792–803. https://doi.org/10.1080/01490451.2011.619640

Mitchell, A. C., Lafrenière, M. J., Skidmore, M. L., & Boyd, E. S. (2013). Influence of bedrock mineral composition on microbial diversity in a subglacial environment. *Geology*, *41*(8), 855–858. https://doi.org/10.1130/G34194.1

Montross, S. N., Skidmore, M., Tranter, M., Kivimäki, A.-L., & Parkes, R. J. (2013). A microbial driver of chemical weathering in glaciated systems. *Geology*, *41*(2), 215–218. https://doi.org/10.1130/G33572.1

Moore, E. R. B., Tindall, B. J., Martins Dos Santos, V. A. P., Pieper, D. H., Ramos, J.-L., & Palleroni, N. J. (2006). Nonmedical: Pseudomonas. In M. Dworkin, S. Falkow, E. Rosenberg, K.-H. Schleifer, & E. Stackebrandt (Eds.), *The Prokaryotes: Volume 6: Proteobacteria: Gamma subclass* (pp. 646–703). Springer.

Moses, C. O., & Herman, J. S. (1991). Pyrite oxidation at circumneutral pH. *Geochimica Et Cosmochimica Acta*, *55*(2), 471–482. https://doi.org/10.1016/0016-7037(91)90005-P

Moses, C. O., Kirk Nordstrom, D., Herman, J. S., & Mills, A. L. (1987). Aqueous pyrite oxidation by dissolved oxygen and by ferric iron. *Geochimica Et Cosmochimica Acta*, *51*(6), 1561–1571. https://doi.org/10.1016/0016-7037(87)90337-1

Napieralski, S. A., Buss, H. L., Brantley, S. L., Lee, S., Xu, H., & Roden, E. E. (2019). Microbial chemolithotrophy mediates oxidative weathering of granitic bedrock. *Proceedings of the National Academy of Sciences of the United States of America*, *116*(52), 26394–26401. https://doi.org/10.1073/pnas.1909970117

Napieralski, S. A., & Roden, E. E. (2020). The weathering microbiome of an outcropping granodiorite. *Frontiers in Microbiology*, *11*, 601907. https://doi.org/10.3389/fmicb.2020.601907

Nicholson, R. V., Gillham, R. W., & Reardon, E. J. (1988). Pyrite oxidation in carbonate-buffered solution: 1. Experimental kinetics. *Geochimica Et Cosmochimica Acta*, *52*(5), 1077–1085. https://doi.org/10.1016/0016-7037(88)90262-1

Nor, Y. M., & Tabatabai, M. A. (1975). Colorimetric determination of microgram quantities of thiosulfate and tetrathionate. *Analytical Letters*, *8*(8), 537–547. https://doi.org/10.1080/00032717508058238

Parge, H. E., Forest, K. T., Hickey, M. J., Christensen, D. A., Getzoff, E. D., & Tainer, J. A. (1995). Structure of the fibre-forming protein pilin at 2.6 Å resolution. *Nature*, *378*(6552), 32–38. https://doi.org/10.1038/378032a0

Parks, D. H., Imelfort, M., Skennerton, C. T., Hugenholtz, P., & Tyson, G. W. (2015). CheckM: assessing the quality of microbial genomes recovered from isolates, single cells, and metagenomes. *Genome Research*, *25*(7), 1043–1055. https://doi.org/10.1101/gr.186072.114

Peabody, C. R., Chung, Y. J., Yen, M.-R., Vidal-Ingigliardi, D., Pugsley, A. P., & Saier, M. H. (2003). Type II protein secretion and its relationship to bacterial type IV pili and archaeal flagella. *Microbiology*, *149*(Pt 11), 3051–3072. https://doi.org/10.1099/mic.0.26364-0

Percak-Dennett, E., He, S., Converse, B., Konishi, H., Xu, H., Corcoran, A., Noguera, D., Chan, C., Bhattacharyya, A., Borch, T., Boyd, E., & Roden, E. E. (2017). Microbial acceleration of aerobic pyrite oxidation at circumneutral pH. *Geobiology*, *15*(5), 690–703.

Peretyazhko, T. S., Zachara, J. M., Kukkadapu, R. K., Heald, S. M., Kutnyakov, I. V., Resch, C. T., Arey, B. W., Wang, C. M., Kovarik, L., Phillips, J. L., & Moore, D. A. (2012). Pertechnetate (TcO_4^-) reduction by reactive ferrous iron forms in naturally anoxic, redox transition zone sediments from the Hanford Site, USA. *Geochimica Et Cosmochimica Acta*, *92*, 48–66. https://doi.org/10.1016/j.gca.2012.05.041

Pichler, T., & Veizer, J. (1999). Precipitation of Fe(III) oxyhydroxide deposits from shallow-water hydrothermal fluids in Tutum Bay, Ambitle Island, Papua New Guinea. *Chemical Geology*, *162*(1), 15–31. https://doi.org/10.1016/S0009-2541(99)00068-6

Pott, A. S., & Dahl, C. (1998). Sirohaem sulfite reductase and other proteins encoded by genes at the dsr locus of *Chromatium vinosum* are involved in the oxidation of intracellular sulfur. *Microbiology*, *144*(7), 1881–1984. https://doi.org/10.1099/00221287-144-7-1881

Quast, C., Pruesse, E., Yilmaz, P., Gerken, J., Schweer, T., Yarza, P., Peplies, J., & Glöckner, F. O. (2013). The SILVA ribosomal RNA gene database project: Improved data processing and web-based tools. *Nucleic Acids Research*, *41*(Database issue), D590–D596. https://doi.org/10.1093/nar/gks1219

Raiswell, R., & Canfield, D. E. (2012). The iron biogeochemical cycle past and present. *Geochemical Perspectives*, *1*(1), 1–232. https://doi.org/10.7185/geochempersp.1.1

Rohwerder, T., & Sand, W. (2003). The sulfane sulfur of persulfides is the actual substrate of the sulfur-oxidizing enzymes from *Acidithiobacillus* and *Acidiphilium* spp. *Microbiology*, *149*(Pt 7), 1699–1710. https://doi.org/10.1099/mic.0.26212-0

Rondelet, A., & Condemine, G. (2013). Type II secretion: The substrates that won't go away. *Research in Microbiology*, *164*(6), 556–561. https://doi.org/10.1016/j.resmic.2013.03.005

Sauvonnet, N., Vignon, G., Pugsley, A. P., & Gounon, P. (2000). Pilus formation and protein secretion by the same machinery in Escherichia coli. *EMBO*, *19*(10), 2221–2228. https://doi.org/10.1093/emboj/19.10.2221

Schippers, A., Breuker, A., Blazejak, A., Bosecker, K., Kock, D., & Wright, T. L. (2010). The biogeochemistry and microbiology of sulfidic mine waste and bioleaching dumps and heaps, and novel Fe(II)-oxidizing bacteria. *Hydrometallurgy*, *104*(3–4), 342–350. https://doi.org/10.1016/j.hydromet.2010.01.012

Schippers, A., Von Rège, H., & Sand, W. (1996). Impact of microbial diversity and sulfur chemistry on safeguarding sulfudic mine waste. *Minerals Engineering*, *9*(10), 1069–1079. https://doi.org/10.1016/0892-6875(96)00099-4

Seemann, T. (2014). Prokka: rapid prokaryotic genome annotation. *Bioinformatics*, *30*(14), 2068–2069. https://doi.org/10.1093/bioinformatics/btu153

Shi, L., Deng, S., Marshall, M. J., Wang, Z., Kennedy, D. W., Dohnalkova, A. C., Mottaz, H. M., Hill, E. A., Gorby, Y. A., Beliaev, A. S., Richardson, D. J., Zachara, J. M., & Fredrickson, J. K. (2008). Direct involvement of type II secretion system in extracellular translocation of *Shewanella oneidensis* outer membrane cytochromes MtrC and OmcA. *Journal of Bacteriology*, *190*(15), 5512–5516.

Singer, P. C., & Stumm, W. (1970). Acidic mine drainage : The rate-determining step. *Science*, *167*(3921), 1121–1123.

Skidmore, M., Anderson, S. P., Sharp, M., Foght, J., & Lanoil, B. D. (2005). Comparison of microbial community compositions of two subglacial environments reveals a possible role for microbes in chemical weathering processes. *Applied and Environment Microbiology*, *71*(11), 6986–6997. https://doi.org/10.1128/AEM.71.11.6986-6997.2005

Stookey, L. L. (1970). Ferrozine-Anew spectrophotometric reagent for iron. *Analytical Chemistry*, *42*(7), 778–781. https://doi.org/10.1021/ac60289a016

Sullivan, P. L., Hynek, S. A., Gu, X., Singha, K., White, T., West, N., Kim, H., Clarke, B., Kirby, E., Duffy, C., & Brantley, S. L. (2016). Oxidative dissolution under the channel leads geomorphological evolution at the Shale Hills catchment. *American Journal of Science*, *316*(10), 981–1026. https://doi.org/10.2475/10.2016.02

Sullivan, P. L., Ma, L., West, N., Jin, L., Karwan, D. L., Noireaux, J., Steinhoefel, G., Gaines, K. P., Eissenstat, D. M., Gaillardet, J., Derry, L. A., Meek, K., Hynek, S., & Brantley, S. L. (2016). CZ-tope at Susquehanna Shale Hills CZO: Synthesizing multiple isotope proxies to elucidate Critical Zone processes across timescales in a temperate forested landscape. *Chemical Geology*, *445*, 103–119. https://doi.org/10.1016/j.chemgeo.2016.05.012

Swedlund, P. J., & Webster, J. G. (1999). Adsorption and polymerisation of silicic acid on ferrihydrite, and its effect on arsenic adsorption. *Water Research*, *33*(16), 3413–3422. https://doi.org/10.1016/S0043-1354(99)00055-X

Turner, B. F., Stallard, R. F., & Brantley, S. L. (2003). Investigation of in situ weathering of quartz diorite bedrock in the Rio Icacos basin, Luquillo Experimental Forest. *Puerto Rico. Chemical Geology*, *202*(3–4), 313–341. https://doi.org/10.1016/j.chemgeo.2003.05.001

Tuttle, J. H., & Jannasch, H. W. (1976). Microbial utilization of thiosulfate in the deep sea. *Limnology and Oceanography*, *21*(5), 697–701.

Uritskiy, G. V., DiRuggiero, J., & Taylor, J. (2018). MetaWRAP-a flexible pipeline for genome-resolved metagenomic data analysis. *Microbiome*, *6*(1), 158. https://doi.org/10.1186/s40168-018-0541-1

Vear, A., & Curtis, C. (1981). A quantitative evaluation of pyrite weathering. *Earth Surface Processes and Landforms*, *6*(2), 191–198. https://doi.org/10.1002/esp.3290060214

Watanabe, T., Kojima, H., Umezawa, K., Hori, C., Takasuka, T. E., Kato, Y., & Fukui, M. (2019). Genomes of neutrophilic sulfur-oxidizing chemolithoautotrophs representing 9 proteobacterial species from 8 genera. *Frontiers in Microbiology*, *10*, 316. https://doi.org/10.3389/fmicb.2019.00316

Wirsen, C. O., Jannasch, H. W., & Molyneaux, S. J. (1993). Chemosynthetic microbial activity at Mid-Atlantic Ridge hydrothermal vent sites. *Journal of Geophysical Research*, *98*(B6), 9693. https://doi.org/10.1029/92JB01556

Wu, Y.-W., Simmons, B. A., & Singer, S. W. (2015). MaxBin 2.0: An automated binning algorithm to recover genomes from multiple metagenomic datasets. *Bioinformatics*, *32*(4), 605–607. https://doi.org/10.1093/bioinformatics/btv638

Yan, R., Kappler, A., Muehe, E. M., Knorr, K.-H., Horn, M. A., Poser, A., Lohmayer, R., & Peiffer, S. (2019). Effect of reduced sulfur species on chemolithoautotrophic pyrite oxidation with nitrate. *Geomicrobiology Journal*, *36*(1), 19–29. https://doi.org/10.1080/01490451.2018.1489915

Yin, H., Zhang, X., Li, X., He, Z., Liang, Y., Guo, X., Hu, Q. I., Xiao, Y., Cong, J., Ma, L., Niu, J., & Liu, X. (2014). Whole-genome sequencing reveals novel insights into sulfur oxidation in the extremophile *Acidithiobacillus thiooxidans*. *BMC Microbiology*, *14*, 179. https://doi.org/10.1186/1471-2180-14-179

Yu, C. S., Chen, Y. C., Lu, C. H., & Hwang, J. K. (2006). Prediction of protein subcellular localization. *Proteins*, *64*(3), 643–651. https://doi.org/10.1002/prot.21018

Zhou, J., Bruns, M. A., & Tiedje, J. M. (1996). DNA recovery from soils of diverse composition. *Applied and Environmental Microbiology*, *62*(2), 316–322. https://doi.org/10.1128/aem.62.2.316-322.1996

Zhu, W., & Reinfelder, J. R. (2012). The microbial community of a black shale pyrite biofilm and its implications for pyrite weathering. *Geomicrobiology Journal*, *29*(2), 186–193. https://doi.org/10.1080/01490451.2010.539663

SUPPORTING INFORMATION

Additional supporting information may be found in the online version of the article at the publisher's website.

How to cite this article: Napieralski, S. A., Fang, Y., Marcon, V., Forsythe, B., Brantley, S. L., Xu, H., & Roden, E. E. (2021). Microbial chemolithotrophic oxidation of pyrite in a subsurface shale weathering environment: Geologic considerations and potential mechanisms. *Geobiology*, 00, 1–21. https://doi.org/10.1111/gbi.12474